Bioorganic & Medicinal Chemistry 17 (2009) 4916–4920

Contents lists available at ScienceDirect

Bioorganic & Medicinal Chemistry

journal homepage: www.elsevier.com/locate/bmc

Design and synthesis of membrane fusion inhibitors against the feline immunodeficiency virus

Shinya Oishi [a,*], Yasuyo Kodera [a], Hiroki Nishikawa [a], Hirotaka Kamitani [a], Tsuyoshi Watabe [a], Hiroaki Ohno [a], Tadafumi Tochikura [a], Kazuki Shimane [b], Eiichi Kodama [b,†], Masao Matsuoka [b], Fuminori Mizukoshi [c], Hajime Tsujimoto [c], Nobutaka Fujii [a,*]

[a] Graduate School of Pharmaceutical Sciences, Kyoto University, Sakyo-ku, Kyoto 606-8501, Japan
[b] Laboratory of Virus Control, Institute for Virus Research, Kyoto University, Sakyo-ku, Kyoto 606-8507, Japan
[c] Department of Veterinary Internal Medicine, Graduate School of Agricultural and Life Sciences, The University of Tokyo, 1-1-1 Yayoi, Bunkyo-ku, Tokyo 113-8657, Japan

ARTICLE INFO

Article history:
Received 24 April 2009
Revised 30 May 2009
Accepted 2 June 2009
Available online 6 June 2009

Keywords:
Feline immunodeficiency virus
Fusion inhibitor
α-Helix
Heptad repeat

ABSTRACT

Feline immunodeficiency virus (FIV) is a pathogenic virus that causes an AIDS-like syndrome in the domestic cats. For viral entry and infection, fusion between the virus and the cell membrane is the critical process and this process is mediated by an envelope glycoprotein gp40. We have identified fusion inhibitory peptides from the heptad repeat-2 (HR2) of gp40. Remodeling of the original sequences using α-helix-inducible motifs revealed the interactive residues of gp40. Comparative analysis of HR2 peptides derived from four FIV strains demonstrated that the interactive surface of the Shizuoka strain-derived HR2 peptides provides the highest affinity of all the FIV strains examined.

1. Introduction

Feline immunodeficiency virus (FIV) causes immunodeficiency in domestic cats. The prevalence is very high in many countries.[1] FIV shares a homologous replication cycle and pathological processes with human immunodeficiency virus (HIV) in which a progressive and irreversible depletion of $CD4^+$ T cells leads to an AIDS-like syndrome. FIV is horizontally transmitted by the exposure to virus contained in blood or saliva from infected cats and it can be vertically transmitted from queens to kittens, sharing similar transmission routes with HIV. Consequently, FIV has been used as an animal model for the development of anti-HIV agents.[2]

The cell entry process of viruses including receptor binding and membrane fusion is mediated by the envelope glycoproteins.[3] In the initial stage for productive infection, the FIV surface (SU) glycoprotein attaches to both CD134 and CXCR4.[4] The primary receptor of FIV is CD134 expressed on activated $CD4^+$ T cells in contrast that the primate lentiviruses target CD4. The co-receptor CXCR4 is targeted both by FIV and HIV.[5] The inhibitors of this process such as specific CXCR4 antagonists effectively suppress viral replication.[5b,6] Fusion between the host cellular and viral membranes occurs through the rearrangement of the transmembrane (TM) glycoprotein gp40.[7] Although the detailed mechanism of the fusion process of FIV remains unresolved, the conservation of the gp40 ectodomain among the lentiviruses supports the class I membrane fusion reaction. The folding of two heptad repeats in gp40 leads to the formation of a trimer of hairpins with a central α-helical coiled-coil that promotes membrane fusion. As recently observed in the successful development of an HIV fusion inhibitor, enfuvirtide,[8] the fusion process is another promising target for anti-FIV agents.[9]

Recently, we have reported the identification of two potent HIV fusion inhibitors by the remodeling of HIV-1 gp41-derived peptides.[10] Both peptides were designed by the stabilization of bioactive α-helical conformations of C34 **1** and enfuvirtide, which inhibit the refolding process to produce the fusogenic six-helix bundle structure. Incorporation of the characteristic X–EE–XX–KK repeats (X: the original residue; E: Glu; K: Lys) into the gp41 heptad repeat-2 (HR2) peptides stabilized the α-helix structure by the formation of potential electrostatic interaction between Glu at the *i* position and Lys at the *i* + 4 position. Such peptide stabilization resulted in improved anti-HIV activity. In addition, this approach simultaneously distinguished the indispensable residues located at the interactive surface from the less essential solvent accessible residues. These residues can be substituted for improving the aqueous solubility of the peptides. We speculate that this design

* Corresponding authors. Tel.: +81 75 753 4551; fax: +81 75 753 4570.
E-mail addresses: soishi@pharm.kyoto-u.ac.jp (S. Oishi), nfujii@pharm.kyoto-u.ac.jp (N. Fujii).
† Present address: Division of Emerging Infectious Diseases, Tohoku University School of Medicine, 2-1 Seiryocho, Aoba-ku, Sendai 980-8575, Japan.

0968-0896/$ - see front matter © 2009 Elsevier Ltd. All rights reserved.
doi:10.1016/j.bmc.2009.06.001

concept should be applicable to anti-FIV peptides. Since there have been no previous reports on the interactive mode of FIV gp40 during the fusion process, this approach could identify novel potent anti-FIV peptides and disclose the interacting interface for further optimization.

Herein, we present the design, synthesis and bioevaluation of FIV HR2-derived peptides with α-helix inducible motifs. On the basis of the appropriate anti-FIV sequence identified, the congeneric HR2 peptides from four FIV strains belonging to two different subtypes were comparatively evaluated for inhibitory activity against the fusion process by using an ELISA.

2. Results and discussion

2.1. Peptide design and synthesis

Peptide design began with two putative coiled-coil-like regions of FIV envelope protein gp40 identified by the LearnCoil-VMF program.[11] Alignment with two heptad repeats of HIV-1 gp41 identified the corresponding heptad repeat-1 (HR1) and HR2 regions in FIV gp40 (Fig. 1a).[11] The predicted C-terminal sequence **3a** coincides with a previously reported effective inhibitor of FIV infection, T1577,[9b] and shares four amino acids with HR2 of HIV-1 gp41. The potential α-helical wheel of **3a** is depicted in Figure 1b. On the basis of the crystal structure of HIV-1 gp41 and the alignment with the HIV-1 sequence, it is assumed that residues at the *a*, *d* and *e* positions of peptide **3a** are involved in the interaction with the central coiled-coil of the HR1 trimer to form the six-helix bundle. On the other hand, residues at *b*, *c*, *f* and *g* positions may facilitate the stabilization of the bioactive secondary structure rather than directly interact with HR1. We designed a modified peptide **4a**, in which Glu and Lys were arranged for *b*/*c* and *f*/*g* positions of **3a**, respectively, in order to stabilize the α-helix structure through the formation of consecutive salt bridges. In addition, two analogues **5** and **6** with shifted interactive surfaces were designed, in which *a*/*b*/*e* and *a*/*d*/*g* positions were expected to interact with HR1, respectively.

All peptides were prepared by a standard protocol for Fmoc-based solid-phase peptide synthesis. The peptide resins were manually constructed using *N*,*N*-diisopropylcarbodiimide (DIC) and *N*-hydroxybenzotriazole (HOBt) on NovaSyn TGR resin. The peptide N-terminus was acetylated. The peptides were obtained by the treatment with the deprotection cocktail [TFA/thioanisole/*m*-cresol/1,2-ethanedithiol/H_2O (80:5:5:5:5)] followed by HPLC purification. The peptides were characterized by mass spectrometry.

2.2. Identification of the interactive surface of HR2 for binding with the HR1 core

The inhibitory potency of HR2 peptides against the six-helix bundle formation of FIV gp40 was examined by an ELISA (Table 1).[12] Two peptides **4a** and **5** exhibited higher inhibition compared with the parent peptide **3a** [IC_{50}(**3a**) = 708 nM; IC_{50}(**4a**) = 16.6 nM; IC_{50}(**5**) = 169 nM], whereas peptide **6** did not inhibit the interaction even at 10 μM. HIV fusion inhibitors C34 **1** and SC35EK **2** showed no inhibition. These results indicate that the FIV HR2 sequence may interact with the HR1 coiled-coil via the residues positioned at *a*/*b*/*e* and/or *a*/*d*/*e*. On the other hand, FIV-mediated syncytium formation and FIV replication were blocked by treatment with peptides **3a** and **4a**, but not by peptides **5** and **6**.[13] Inhibition of the HR1–HR2 interaction by peptide **5** did not lead to anti-FIV activity suggesting that residues at *d* position are required for the interaction with HR1 of FIV gp40.

In order to rationalize the relationship between bioactivity and the conformations of the HR2 peptides, circular dichroism (CD) spectra were measured for peptides **3a, 4a, 5** and **6** in the absence or presence of the HR1 peptide. Negative ellipticities around 208 and 222 nm indicate the presence of a stable α-helix structures for peptides **4a** and **5** in the absence of the HR1 peptide (Fig. 2a). In contrast, although the α-helix inducible motifs were included, a random structure was observed for peptide **6**. The CD spectrum

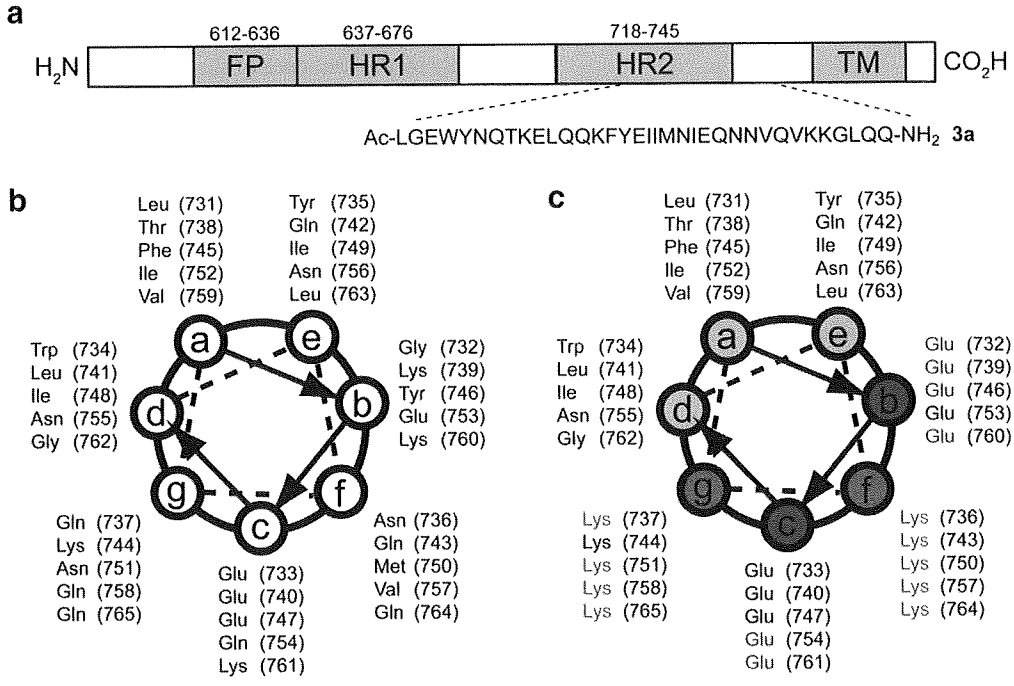

Figure 1. Design of FIV fusion inhibitors. (a) Schematic representation of FIV-1 gp40. The helical wheel representation of the HR2 peptide of FIV-1 gp40: (b) peptide **3a** and (c) peptide **4a**. FP: fusion peptide; HR1: heptad repeat-1; HR2: heptad repeat-2; TM: transmembrane domain.

Table 1
Sequences and bioactivity of HR2-derived peptides of HIV-1 and FIV.

Peptide	Sequence	IC_{50} (nM)[a]
HIV-1		
1 (C34)	WMEWDREINNYTSLIHSLIEESQNQQEKNEQELL	>10,000
2 (SC35EK)	WEEWDKKIEEYTKKIEELIKKSEEQQKKNEEELKK	>10,000
FIV		
3a	LGEWYNQTKELQQKFYEIIMNIEQNNVQVKKGLQQ	708
4a	LEEWYKKTEELQKKFEEIIKKIEENNKKVEEGLKK	16.6
5	NEELGKKYEETKKKQEEFYKKIEEIEKKNEEVKKKLEELQKK	169
6	GEETLKKWEEQTKKLEEKFKKIEENIKKNEEQVKKGEEQLKK	>10,000

[a] IC_{50} was determined as the concentration that blocked HR1–HR2 interaction by 50% in an ELISA.

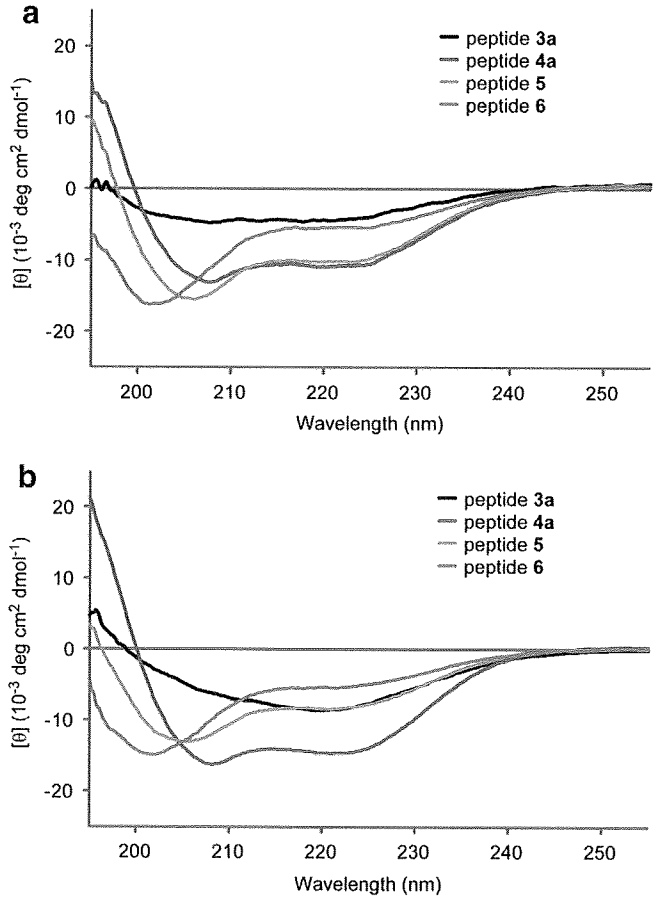

Figure 2. Circular dichroism spectra of HR2 peptides **3a**, **4a**, **5** and **6** in the presence (a) and absence (b) of the HR1 peptide.

of peptide **4a** in the presence of the HR1 peptide showed a slight enhancement of α-helix conformation compared with the theoretical spectrum of the mixture without the interaction between HR1 and HR2 (Fig. 2b). This observation suggests that a stable six-helix bundle structure was formed between HR1 peptide and **4a**. The other HR1–HR2 mixtures did not indicate any enhancement in α-helix content, which is correlated with the results obtained by a replication assay.[13] As such, it was demonstrated that residues at positions *a*/*d*/*e* of peptide **4a** provide the most appropriate interactive surface required for designing inhibitors against FIV infection (Fig. 1c).

2.3. Structure–activity relationship for designing potent fusion inhibitors against multiple FIV strains

The inhibitory potency of the anti-FIV HR2 peptides is affected by both the interactive surface and the stabilized α-helix conformations supported by the arrangement of residues exposed to the aqueous solvent. Since the α-helix content and stability of the peptide was enhanced by the X–EE–XX–KK motifs, the *a*, *d* and *e* positions could be further optimized for improving binding affinity. In addition, considering the clinical application against feline immunodeficiency, inhibitors that potently suppress broad range of FIV strains are favorable. Next, comparative inhibition of analogous peptides **3a–d** (native sequences) and **4a–d** (remodeled sequences) derived from several FIV strains was examined against potential formation of the six-helix bundles (Tables 2 and 3). Noticeably, peptide **3d** from the Shizuoka strain (clade D) contains ten different residues from **3a** (UK8) and **3c** (Sendai-1), and nine from **3b** (Petaluma). In contrast, there are only three differences in residue type observed among remodeled peptides **4a–d**, suggesting that the potential interactive residues are conserved among the four FIV strains.

ELISA with gp40 fragments derived from each strain was performed. Peptides **4a–d** with α-helix inducible motifs exhibited higher potency of inhibition compared with the native sequences **3a–d**. FIV-mediated syncytium formation was also inhibited by peptides **3b** and **4b** (Fig. 3). Sendai-1-derived peptides **3c** and **4c** were less potent compared with the other peptides, suggesting that the N26S substitution on the interactive surface results in a decrease in the affinity towards the HR1 peptide. In contrast, the Shizuoka sequence provided the most potent peptides **3d** and **4d** against all strains. The potent bioactivity was attributed to a combination of Gly and Leu at the positions 29 and 33, respectively. Accordingly, the exposure of appropriate residues on the HR2 interactive surface such as the Shizuoka strain-derived peptide **4d** provide optimized inhibition against the formation of the six-helix bundle.

Comparative CD analysis demonstrated that the sequences of the HR1 peptide apparently influence the structures of the six-helix bundles (Fig. 4a). In contrast, peptides **4a–d** in the presence of an HR1 peptide derived from each strain exhibited similar six-helix bundle structures (Fig. 4b and Supplementary data).[14] These observations suggest that the binding affinity between the viral HR1 peptide and the inhibitory HR2 peptide would be determined primarily by the sequence of the viral HR1 peptide when the HR2 sequence was simplified by the incorporation of α-helix inducible motifs.

Table 2
Sequences of HR2-derived peptides of four FIV strains.

Peptide		Sequence[a]
clade A		1 10 20 30 35
UK8	**3a**	LGEWYNQTKELQQKFYEIIMNIEQNNVQVKKGLQQ
	4a	LEEWYKKTEELQKKFEEIIKKIEENNKKVEEGLKK
Petaluma	**3b**	LGEWYNQTKDLQQKFYEIIMDIEQNNVQGKKGIQQ
	4b	LEEWYKKTEELQKKFEEIIKKIEENNKK EEG KK
Sendai-1	**3c**	LGEWYNQTKGLQQKFYEIIMDIEQNSVQGKKGIQQ
	4c	LEEWYKKTEELQKKFEEIIKKIEEN KK EEG KK
clade D		
Shizuoka	**3d**	LRDWYNNTQQLQKKFYEIIYDIEQNNVQGKQGLQQ
	4d	LEEWYKKTEELQKKFEEIIKKIEENNKK EEGLKK

[a] The different residues in peptides **4b–d** from peptide **4a** are marked in green.

Table 3
Inhibitory activity of HR2-derived peptides against the HR1–HR2 interaction of four FIV strains

Peptide	IC_{50} (nM, ELISA)[a]			
	UK8	Petaluma	Sendai-1	Shizuoka
3a	724	708	646	6310
3b	513	1260	183	6310
3c	>10,000	2400	437	>10,000
3d	182	195	37.2	2510
4a	5.39	16.6	22.6	115
4b	9.33	51.6	8.87	78.5
4c	443	200	42.4	203
4d	3.38	12.8	2.53	19.7

[a] IC_{50} was determined as the concentration that blocked HR1–HR2 interaction by 50% in an ELISA.

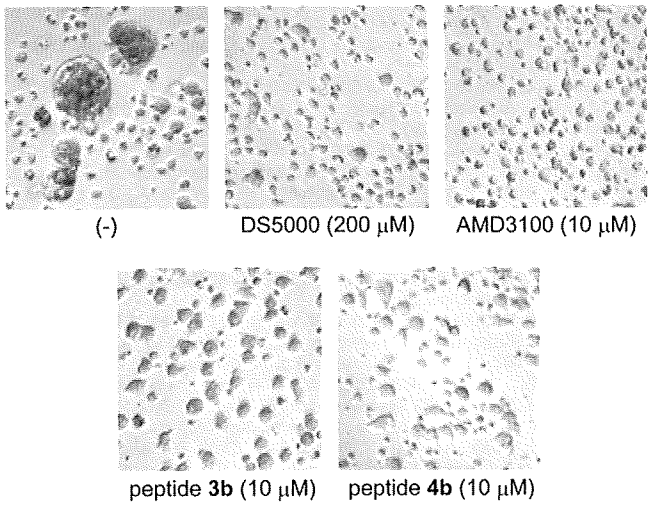

Figure 3. Inhibition of FIV-mediated cell fusion by peptides **3b** and **4b**.

3. Conclusions

The current study investigated the use of an α-helix inducible X–EE–XX–KK motif to stabilize the interaction between HR2 and the HR1 coiled-coil of the FIV gp40 protein. The most appropriate interactive surface on the HR2 peptide to provide potent inhibition appeared in the remodeled peptide **4a**, which was designed on the basis of the alignment with the HIV-1 gp41 HR2 sequence. Comparative analysis of HR2 peptides derived from several strains indicated that the most potent inhibition was provided by the interactive residues of the Shizuoka strain-derived peptide **4d**. As such, replacement of the solvent accessible residues with arranged Glu and Lys residues facilitated the optimization process of the interactive residues for high affinity binding on to the HR1 structure. Since class I virus fusion proteins share a high degree of structural homology and similar molecular mechanisms, the current approach may be useful in designing fusion inhibitors against other related viruses.

4. Experimental

4.1. Peptide synthesis

Protected peptide-resins were manually constructed by Fmoc-based solid-phase peptide synthesis on NovaSyn® TGR resin (0.26 mmol/g, 385 mg, 0.1 mmol). *t*-Bu ester for Asp and Glu; 2,2,4,6,7-pentamethyldihydrobenzofuran-5-sulfonyl (Pbf) for Arg; *t*-Bu for Thr, Tyr and Ser; Boc for Lys; and Trt for Gln, Asn and His were employed for side-chain protection. Fmoc-amino acids were coupled using Fmoc-amino acid (0.5 mmol), *N,N'*-diisopropylcarbodiimide (DIC, 0.077 mL, 0.5 mmol) and HOBt·H_2O (77 mg) in DMF for 1.5 h. Fmoc deprotection was performed with 20% piperidine in DMF for 20 min. After N-terminal acetyl capping by treatment with Ac_2O (0.050 mL)-pyridine (0.050 mL), the protected resin (200 mg) was treated with TFA/thioanisole/*m*-cresol/1,2-ethandithiol/H_2O (80:5:5:5:5, 2.5 mL) at room temperature for 2 h. After removal of the resin by filtration, the filtrate was poured into ice-cold dry Et_2O. The resulting powder was collected by centrifugation and washed with ice-cold dry diethyl ether. Purification of the crude product by preparative HPLC on a Cosmosil 5C18-ARII preparative column (Nacalai Tesque, 20 × 250 mm) afforded the expected peptides. All peptides were characterized by an ESI-MS (Sciex API*III*E, Toronto, Canada) or MALDI-TOF-MS (AXIMA-CFR plus, Shimadzu, Kyoto, Japan), and the purity was calculated as >95% by HPLC on a Cosmosil 5C18-ARII analytical column (Nacalai Tesque, 4.6 × 250 mm) at 220 nm absorbance. The MS data are shown in Supplementary data.

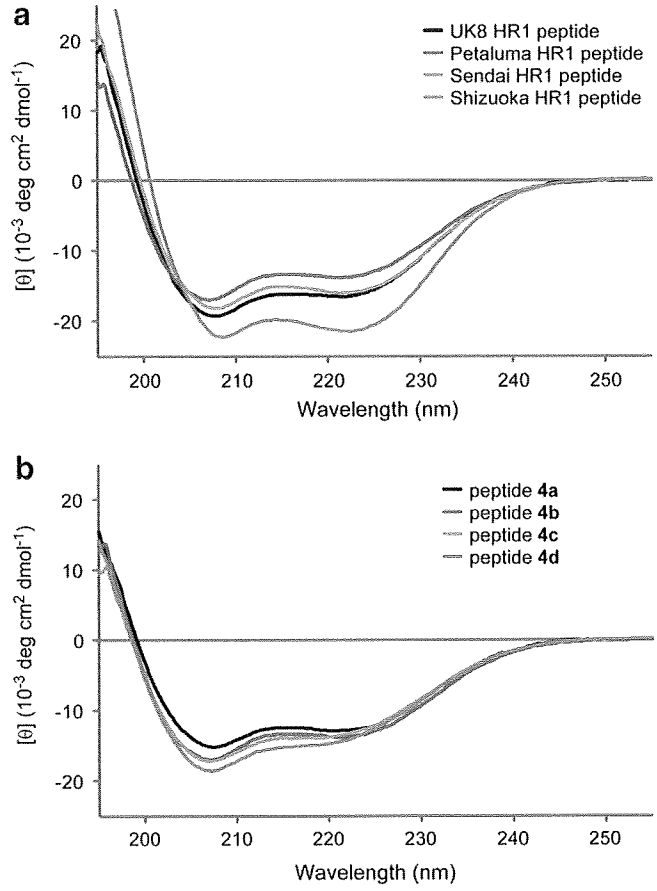

Figure 4. Circular dichroism spectra of (a) peptide **4a** in the presence of HR1 peptides (four strains) and (b) peptides **4a–d** in the presence of the HR1 peptide (Petaluma strain).

4.2. FIV syncytial assay[15]

3201/FIV cells (2 × 10^4 cells/well) and MT-2 cells (1 × 10^3 cells/well) were seeded into 96-well plates with each peptide (10 μM). After 7 days, the cells were fixed with 1% formaldehyde and were examined using a BioZERO microscope (BZ-8000; Keyence, Osaka, Japan).

4.3. ELISA-based competition assay

Recombinant purified MBP-HR1 dissolved in 50 mM sodium carbonate buffer (pH 8.5) was coated on a 96-well ELISA plate

(Costar, Cambridge, MA) by incubation at 4 °C for 12 h. After washing three times with PBS containing 0.25% Tween 20 (T-PBS), the plate was blocked using bovine serum albumin (BSA) at a concentration of 1 mg/mL in T-PBS at 4 °C for 2.5 h, and then washed again as described above. The MBP-HR1 was allowed to bind biotinylated HR2 peptide (peptide **3**, 120 nM) by incubation at 37 °C for 1.5 h in the presence or absence of various concentrations of the test peptides. After washing, binding of biotin-HR2 peptide was detected using streptavidin alkaline phosphatase (CALBIOCHEM) using a 1:5000 dilution at 4 °C for 1 h. Subsequently, this reaction was washed as before, prior to the addition of the phosphatase substrate 5-bromo-4-chloro-3-indolyl phosphate (BCIP) (BluePhos Microwell Phosphatase Substrate; KPL, Gaithersburg, MD). After incubating at room temperature for 25 min, the absorbance at 595 nm was measured using a plate reader (Model 3550, Bio-Rad).

4.4. Measurement of CD spectra

The HR2 peptide was dissolved in PBS (pH 7.4) at a concentration of 10 μM. The mixture of the selected HR1 and HR2 peptides was incubated at 37 °C for 30 min prior to the CD measurement (the final concentration of both HR1 and HR2 peptides was 10 μM in PBS, pH 7.4). The wavelength-dependent molar ellipticity [θ] was monitored at 25 °C as the average of eight scans, and the thermal stability of the HR1 and HR2 mixture was estimated by monitoring the change in the CD signal at 222 nm in a spectropolarimeter (Model J-710; Jasco, Tokyo, Japan). The midpoint of the thermal unfolding transition of each complex was defined as the melting temperature (T_m).

Acknowledgments

This work was supported by the Science and Technology Incubation Program in Advanced Regions from the Japan Science and Technology Agency, Grants-in-Aid for Scientific Research from the Ministry of Education, Culture, Sports, Science, and Technology of Japan, and Health and Labour Sciences Research Grants (Research on HIV/AIDS). H.N. is grateful for the JSPS Research Fellowships for Young Scientists.

Supplementary data

Supplementary data associated with this article can be found, in the online version, at doi:10.1016/j.bmc.2009.06.001.

References and notes

1. Dunham, S. P.; Graham, E. *Vet. Clin. Small Anim. Pract.* **2008**, *38*, 879.
2. Fletcher, N. F.; Brayden, D. J.; Brankin, B.; Callanan, J. J. *Vet. Immunol. Immunopathol.* **2008**, *123*, 134.
3. (a) Wyatt, R.; Sodroski, J. *Science* **1998**, *280*, 1884; (b) Garg, H.; Fuller, F. J.; Tompkins, W. A. *Virology* **2004**, *321*, 274; (c) Elder, J. H.; Sundstrom, M.; De Rozieres, S.; De Parseval, A.; Grant, C. K.; Lin, Y. C. *Vet. Immunol. Immunopathol.* **2008**, *123*, 3.
4. (a) Shimojima, M.; Miyazawa, T.; Ikeda, Y.; McMonagle, E. L.; Haining, H.; Akashi, H.; Takeuchi, Y.; Hosie, M. J.; Willett, B. J. *Science* **2004**, *303*, 1192; (b) De Parseval, A.; Chatterji, U.; Sun, P.; Elder, J. H. *Proc. Natl. Acad. Sci. U.S.A.* **2004**, *101*, 13044.
5. (a) Willett, B. J.; Hosie, M. J.; Neil, J. C.; Turner, J. D.; Hoxie, J. A. *Nature* **1997**, *385*, 587; (b) Richardson, J.; Pancino, G.; Merat, R.; Leste-Lasserre, T.; Moraillon, A.; Schneider-Mergener, J.; Alizon, M.; Sonigo, P.; Heveker, N. *J. Virol.* **1999**, *73*, 3661.
6. (a) Egberink, H. F.; De Clercq, E.; Van Vliet, A. L.; Balzarini, J.; Bridger, G. J.; Henson, G.; Horzinek, M. C.; Schols, D. *J. Virol.* **1999**, *73*, 6346; (b) Mizukoshi, F.; Baba, K.; Goto-Koshino, Y.; Setoguchi-Mukai, A.; Fujino, Y.; Ohno, K.; Tamamura, H.; Oishi, S.; Fujii, N.; Tsujimoto, H. *J. Vet. Med. Sci.* **2009**, *71*, 121.
7. Kielian, M.; Rey, F. A. *Nat. Rev. Microbiol.* **2006**, *4*, 67.
8. Matthews, T.; Salgo, M.; Greenberg, M.; Chung, J.; DeMasi, R.; Bolognesi, D. *Nat. Rev. Drug Discovery* **2004**, *3*, 215.
9. (a) Lombardi, S.; Massi, C.; Indino, E.; La Rosa, C.; Mazzetti, P.; Falcone, M. L.; Rovero, P.; Fissi, A.; Pieroni, O.; Bandecchi, P.; Esposito, F.; Tozzini, F.; Bendinelli, M.; Garzelli, C. *Virology* **1996**, *220*, 274; (b) Medinas, R. J.; Lambert, D. M.; Tompkins, W. A. *J. Virol.* **2002**, *76*, 9079; (c) D'Ursi, A. M.; Giannecchini, S.; Di Fenza, A.; Esposito, C.; Armenante, M. R.; Carotenuto, A.; Bendinelli, M.; Rovero, P. *J. Med. Chem.* **2003**, *46*, 1807; (d) Giannecchini, S.; Di Fenza, A.; D'Ursi, A. M.; Matteucci, D.; Rovero, P.; Bendinelli, M. *J. Virol.* **2003**, *77*, 3724; (e) Giannecchini, S.; Alcaro, M. C.; Isola, P.; Sichi, O.; Pistello, M.; Papini, A. M.; Rovero, P.; Bendinelli, M. *Antiviral Ther.* **2005**, *10*, 671; (f) D'Ursi, A. M.; Giannecchini, S.; Esposito, C.; Alcaro, M. C.; Sichi, O.; Armenante, M. R.; Carotenuto, A.; Papini, A. M.; Bendinelli, M.; Rovero, P. *Chembiochem.* **2006**, *7*, 774.
10. (a) Otaka, A.; Nakamura, M.; Nameki, D.; Kodama, E.; Uchiyama, S.; Nakamura, S.; Nakano, H.; Tamamura, H.; Kobayashi, Y.; Matsuoka, M.; Fujii, N. *Angew. Chem., Int. Ed.* **2002**, *41*, 2937; (b) Oishi, S.; Ito, S.; Nishikawa, H.; Watanabe, K.; Tanaka, M.; Ohno, H.; Izumi, K.; Sakagami, Y.; Kodama, E.; Matsuoka, M.; Fujii, N. *J. Med. Chem.* **2008**, *51*, 388; (c) Nishikawa, H.; Oishi, S.; Fujita, M.; Watanabe, K.; Tokiwa, R.; Ohno, H.; Kodama, E.; Izumi, K.; Kajiwara, K.; Naitoh, T.; Matsuoka, M.; Otaka, A.; Fujii, N. *Bioorg. Med. Chem.* **2008**, *16*, 9184; (d) Nishikawa, H.; Nakamura, S.; Kodama, E.; Ito, S.; Kajiwara, K.; Izumi, K.; Sakagami, Y.; Oishi, S.; Ohkubo, T.; Kobayashi, Y.; Otaka, A.; Fujii, N.; Matsuoka, M. *Int. J. Biochem. Cell Biol.* **2009**, 891; (e) Naito, T.; Izumi, K.; Kodama, E.; Sakagami, Y.; Kajiwara, K.; Nishikawa, H.; Watanabe, K.; Sarafianos, S. G.; Oishi, S.; Fujii, N.; Matsuoka, M. *Antimicrob. Agent Chemother.* **2009**, *53*, 1013.
11. Singh, M.; Berger, B.; Kim, P. S. *J. Mol. Biol.* **1999**, *290*, 1031.
12. Nishikawa, H.; Kodama, E.; Sakakibara, A.; Fukudome, A.; Izumi, K.; Oishi, S.; Fujii, N.; Matsuoka, M. *Antiviral Res.* **2008**, *80*, 71.
13. Mizukoshi, F.; Baba, K.; Goto, Y.; Setoguchi, A.; Fujino, Y.; Ohno, K.; Oishi, S.; Kodera, Y.; Fujii, N.; Tsujimoto, H. *Vet. Microbiol.* **2009**, *136*, 155.
14. The similar thermal stabilities of the potential six-helix bundle structures were also observed. For example, the melting temperatures (T_m) of peptides **4c** and **4d** in the presence of UK8 strain-derived HR1 peptide were 57.1 °C and 54.7 °C, respectively. Unfortunately, we were not able to get clearer physicochemical proofs of the lower bioactivity of the Sendai strain-derived peptide **4c**.
15. Tanabe-Tochikura, A.; Tochikura, T. S.; Blakeslee, J. R., Jr.; Olsen, R. G.; Mathes, L. E. *Antiviral. Res.* **1992**, *19*, 161.

doi:10.1016/j.jmb.2009.07.027 J. Mol. Biol. (2009) 392, 657–665

JMB

Available online at www.sciencedirect.com

ScienceDirect

ELSEVIER

X-ray Crystallographic Study of an HIV-1 Fusion Inhibitor with the gp41 S138A Substitution

Tsuyoshi Watabe[1], Yukihiro Terakawa[1], Kentaro Watanabe[1], Hiroaki Ohno[1], Hiroaki Nakano[1], Toru Nakatsu[1], Hiroaki Kato[1], Kazuki Izumi[2], Eiichi Kodama[2], Masao Matsuoka[2], Kazuo Kitaura[1], Shinya Oishi[1]* and Nobutaka Fujii[1]*

[1]*Graduate School of Pharmaceutical Sciences, Kyoto University, Sakyo-ku, Kyoto 606-8501, Japan*

[2]*Institute for Virus Research, Kyoto University, Sakyo-ku, Kyoto 606-8507, Japan*

Received 28 March 2009; received in revised form 6 July 2009; accepted 8 July 2009
Available online 17 July 2009

Edited by I. Wilson

The S138A substitution of fusion inhibitory peptides derived from the C-terminal heptad repeat (C-HR) of the human immunodeficiency virus type 1 (HIV-1) gp41 leads to enhanced binding affinity to the N-terminal heptad repeat (N-HR). As such, these peptides exhibit highly potent anti-HIV-1 activity. X-ray crystallographic analysis was performed to understand the effect of the substitution on binding affinity. The comparison of the native and S138A crystal structures indicated that the increase in the hydrophobicity of the S138A substitution may aid the stabilization of the N-HR/C-HR complex through additional hydrophobic contacts. Free-energy calculations suggest that the difference between the desolvation free energies of the C-HR-derived peptides with and without the S138A mutation dominates the observed difference in anti-HIV-1 activity.

Keywords: HIV-1 fusion inhibitor; C-HR-derived peptide; gp41/S138A substitution; hydrophobicity; desolvation energy

Introduction

The entry of human immunodeficiency virus type 1 (HIV-1) into host cells is mediated by the formation of the six-helix bundle of the envelope glycoprotein gp41 consisting of several functional domains (Fig. 1), including the N-terminal heptad repeat (N-HR) and C-terminal heptad repeat (C-HR).[1–4] The N-HR trimeric core of the six-helix bundle has been an attractive anti-HIV drug target. Currently, synthetic peptides derived from the C-HR have been shown to be inhibitors against HIV-1 infection.[5–8] One of these peptides, T-20 (enfuvirtide, Fuzeon; corresponding to residues 127 to 162 of the gp41 C-HR), is an approved anti-HIV-1 peptide for clinical use.[8,9] T-20 inhibits HIV-1 entry into host cells and is used as an alternative anti-HIV drug for patients with drug resistance to reverse transcriptase and/or protease inhibitors. However, long-term therapy with T-20 has led to the emergence of T-20-resistant HIV-1 strains containing mutations within the N- and C-HRs of gp41.[10–12] Consequently, the continuous discovery and development of anti-HIV-1 peptides are essential to overcome drug-resistant HIV-1 strains.

Previously, on the basis of the amino acid sequences of C-HR-derived peptides C34 (corresponding to residues 117 to 150 of gp41 C-HR) and T-20, we designed SC35EK and T-20EK as potent HIV-1 fusion inhibitors against wild-type and T-20-resistant HIV-1 strains.[13,14] Here, N-HR/C-HR interfacial residues critical for interaction with the hydrophobic groove of the N-HR trimeric core were preserved, while other residues were replaced with Glu or Lys to strengthen the bioactive α-helix structure via the formation of potential salt bridges. Other groups have reported that C-HR-derived peptides containing various α-helix-inducible motifs increase peptide bioactivity.[15,16] Although these studies have been successful in producing potent HIV-1 fusion inhibitors, the precise structural analysis are required for improving the N-HR/C-

*Corresponding authors. E-mail addresses: soishi@pharm.kyoto-u.ac.jp; nfujii@pharm.kyoto-u.ac.jp.

Abbreviations used: HIV-1, human immunodeficiency virus type 1; N-HR, N-terminal heptad repeat; C-HR, C-terminal heptad repeat; MAGI, multinuclear activation of the galactosidase indicator; MM, molecular mechanics; PBSA, Poisson–Boltzmann surface area; PDB, Protein Data Bank.

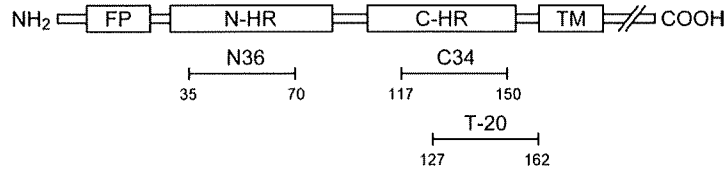

N36: SGIVQQQNNLLRAIEAQQHLLQLTVWGIKQLQARIL

C34: WMEWDREINNYTSLIHSLIEESQNQQEKNEQELL

T-20: YTSLIHSLIEESQNQQEKNEQELLELDKWASLWNWF

Fig. 1. Schematic representation of HIV-1 gp41 (FP, fusion peptide region; TM, transmembrane domain). Peptides N36, C34, and T-20 correspond to residues 35–70, 117–150, and 127–162, respectively. The residues are numbered starting at the first amino acid of the NL4-3 (GIV) gp41.

HR interactions and further peptide and/or non-peptide drug developments.

Currently, the structure–activity relationship studies of an N-HR/C-HR interfacial residue Trp120 in the C-HR-derived peptide C34 were carried out *in vitro* and *in silico*.[17,18] These studies serve as a useful basis for rational drug design targeting the conserved hydrophobic pocket of the N-HR trimeric core. In addition, we have performed an *in vitro* structure–activity relationship study of another residue (i.e., Ser138) located within the N-HR/C-HR binding interface using the C-HR-derived peptides T-20 and C34.[19] Ser138 has been identified to interact within the neighborhood of the primary T-20-resistant mutation region (Leu33-Leu45 of the N-HR), and chemical modification of this residue should improve binding with the T-20-resistant N-HR mutants. We demonstrated that mutation of Ser138 with a small or hydrophobic amino acid enhanced T-20 activity against the wild-type HIV-1. Moreover, the substitution to Ala ($T\text{-}20_{S138A}$) inhibited replication of T-20-resistant clones ($HIV\text{-}1_{V38A}$, $HIV\text{-}1_{N43D}$, and $HIV\text{-}1_{N43D/S138A}$) as efficiently as the wild-type HIV-1. In this article, we have determined the X-ray crystal structure of the $N36/C34_{S138A}$ complex to compare this structure with the previously reported structure of the N36/C34 complex [Protein Data Bank (PDB) code: 1AIK] and evaluate the effect of the S138A substitution. Based on the X-ray coordinates, the binding energies of C34 and $C34_{S138A}$ to the gp41 N-HR were calculated using molecular mechanics (MM) and Poisson–Boltzmann surface area (PBSA) solvation modeling.[20]

Results and Discussion

Anti-HIV-1 activities and thermal stabilities of C-HR-derived peptides

Anti-HIV-1 activities of C-HR-derived peptides (C34 and $C34_{S138A}$) against laboratory HIV-1 NL4-3 (GIV) were evaluated using the multinuclear activation of the galactosidase indicator (MAGI) assay (Table 1).[19] Although original NL4-3 contains D36 substitution,[21] vast majority of HIV-1 strains do G36. Therefore, we used NL4-3(GIV) clone in this study. $C34_{S138A}$ exhibited approximately 4-fold greater anti-HIV-1 activity than C34 [C34, 50% effective concentration (EC_{50}) = 7.3±2.5 nM; $C34_{S138A}$, EC_{50} = 2.0±0.4 nM]. Consequently, the S138A substitution enhanced the C34 activity against the HIV-1 NL4-3(GIV) strain.

The anti-HIV-1 activities of the C-HR-derived peptides have been reported to directly correlate with the apparent melting temperatures (T_m) for the N-HR/C-HR complexes.[17,22,23] As shown in Table 1, the complex containing the $C34_{S138A}$ peptide exhibited a higher T_m value than the complex containing the C34 peptide (N36/C34, T_m = 67.6 °C; N36/$C34_{S138A}$, T_m = 73.2 °C). This observation is in agreement with previous results examining C-HR-derived peptides.

Experimental binding energies (ΔG_{bind} exptl) of the C-HR-derived peptides to the gp41 N-HR have been estimated using the IC_{50} values via ΔG_{bind} exptl $\approx RT\ln(IC_{50})$.[17,18] A 4-fold difference of the IC_{50} values corresponds to a binding energy difference of approximately 1 kcal/mol. As such, the binding energy of $C34_{S138A}$ for the gp41 N-HR was approximately 1 kcal/mol more favorable than that of the binding of C34 to N-HR. Such a small energy difference should play a critical role in increasing/decreasing the anti-HIV-1 activity. Hence, we performed comparative X-ray crystallographic studies on the drug/receptor model complexes of N36/C34 and $N36/C34_{S138A}$ in an effort to understand this energy difference.

Crystallographic study of the six-helix bundle structure with the S138A substitution

The crystal structure of the $N36/C34_{S138A}$ complex is shown in Fig. 2. The crystallographic data are summarized in Table 2. The crystal was indexed to space group *P*321 with unit cell dimensions of $a = b = 49.09$ Å, $c = 56.40$ Å, $\alpha = \beta = 90°$, and $\gamma = 120°$. The structure of the $N36/C34_{S138A}$ complex is a six-helix bundle and is similar to the previously

Table 1. Anti-HIV-1 activities of C-HR-derived peptides against HIV-1 NL4-3(GIV) and thermal stabilities of the six-helix bundles

	EC_{50} (nM)[a]	T_m (°C)[b]
C34	7.3±2.5	67.6
$C34_{S138A}$	2.0±0.4	73.2

[a] EC_{50} was determined as the concentration that blocked HIV-1 replication by 50% in MAGI assay.

[b] Thermal melting temperatures of 10 μM $N36/C34_{S138X}$ complexes (X = S or A).

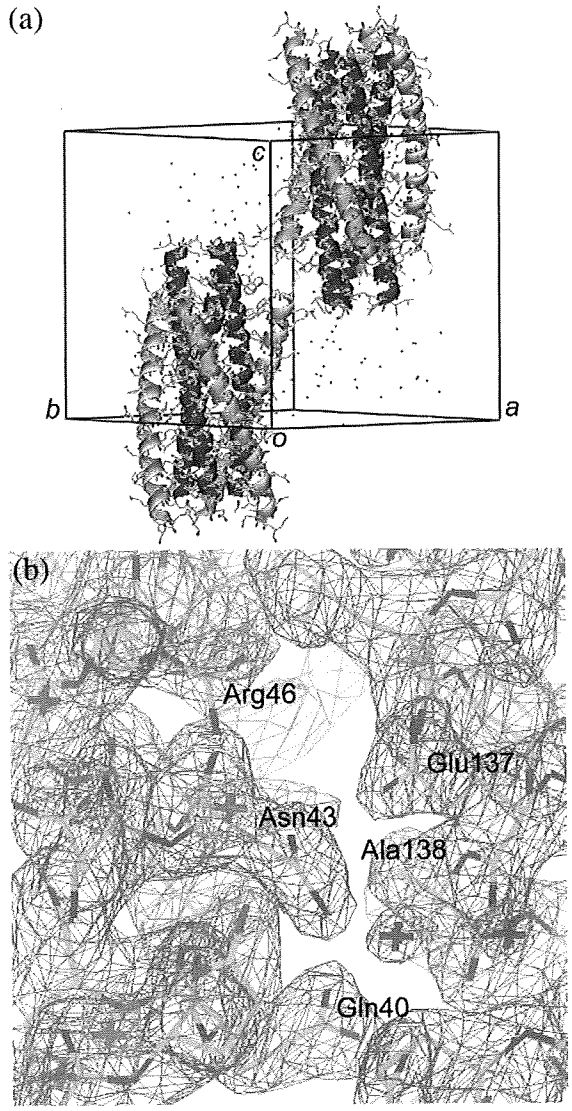

Fig. 2. (a) Crystal structure of the N36/C34$_{S138A}$ complex. N36 and C34$_{S138A}$ helices are colored green and yellow, respectively. (b) Experimental electron density map of the N36/C34$_{S138A}$ complex. The map is contoured at the 1.0 σ level.

reported N36/C34 complex (the C_α RMSD of the two structures is 0.43 Å). The center of this bundle consists of a parallel coiled-coil trimer of the N36 peptides. Three C34$_{S138A}$ peptides wrap in an antiparallel fashion around the outside of the central coiled coil of the N36 peptides. In addition, similar to the N36/C34 complex, the side chain of residue Ala138 packs into the hydrophobic groove and is surrounded by Leu44 and Leu45 of the N36 peptides. Moreover, as shown in Fig. 3, other side chains (Gln40, Asn43, Leu44, Leu45, Glu137, and Gln139) located around residue 138 are near identical in conformation to the N36/C34 complex (the side-chain atom RMSD of the two structures: Gln40, 0.35 Å; Asn43, 0.60 Å; Leu44, 0.34 Å; Leu45, 0.42 Å; Glu137, 0.37 Å; Gln139, 0.85 Å). On the other hand, Arg46 has 1.30 Å side-chain atom RMSD, and

Table 2. Crystallographic data for the N36/C34$_{S138A}$ complex (PDB code: 2ZZO)

Space group	*P*321
Cell parameters	
a, *b*, *c* (Å)	49.09, 49.09, 56.40
α, β, γ (°)	90, 90, 120
Data collection	
Resolution range (Å)	33.95–2.20 (2.28–2.20)
Total number of reflections	43,015
Number of unique reflections	4248
Completeness (%)	99.8 (100.0)
Redundancy	10.13 (9.63)
$I/\sigma(I)$	19.1 (4.3)
R_{merge} (%)	6.1 (40.6)
Wavelength (Å)	1.5418
Model and refinement statistics	
Resolution range (Å)	18.52–2.20
Number of used reflections	4037
Number of atoms (non-H)	
Protein	593
Water	27
Mean *B* value (Å^2)	40.7
RMSD bond lengths (Å)	0.026
RMSD bond angles (°)	2.060
R-factor (%)[a]	21.2
R_{free} (%)[b]	28.3
Ramachandran plot (%)	
Most favored	100.0
Allowed	0.0
Generously allowed	0.0
Disallowed	0.0

[a] *R*-factor is a formula for estimating errors in the data set. *R*-factor = $\sum | F_{obs} - F_{calc} | / \sum | F_{obs} |$; F_{obs} and F_{calc} are the observed and calculated structure-factor amplitudes, respectively.
[b] R_{free} is calculated using an unrefined subset of reflection data.

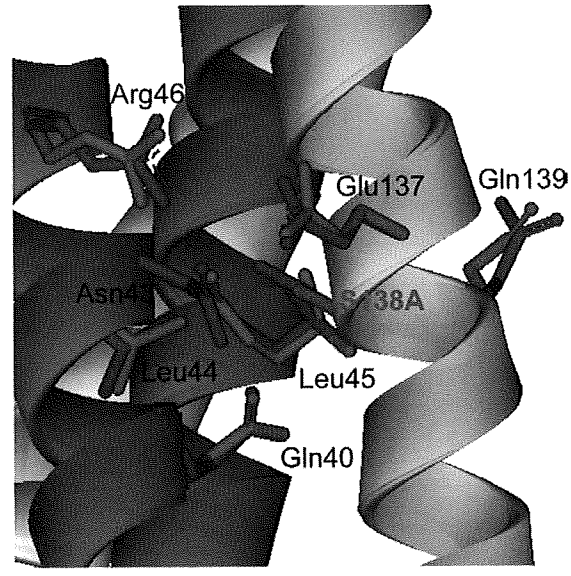

Fig. 3. Superposition of the crystal structure of the N36/C34 complex (PDB code: 1AIK) with that of the N36/C34$_{S138A}$ complex. N36 and C34$_{S138X}$ (X=S or A) helices are colored green and yellow, respectively. In addition, the stick-model side chains (Gln40, Asn43, Leu44, Leu45, Arg46, Glu137, Ser138/Ala138, and Gln139) of N36/C34 and N36/C34$_{S138A}$ are colored blue and red, respectively.

its salt bridge with Glu137 is weakened or broken by the S138A substitution (the distance between the guanidinium group of Arg46 and the carboxyl group of Glu137 is widened from 3.6 to 4.2 Å). These observations indicate that the difference involving the interactions of Ser138 and Ala138 in the C-HR with the hydrophobic groove of N-HR as well as the resulting weakened interaction between Arg46 and Glu137 may influence the N-HR/C-HR complex stability, which relates to the anti-HIV-1 activity.

Currently, based on the X-ray crystal structure of the N36/C34 complex (PDB code: 1AIK), it has been proposed that the S138A substitution increases hydrophobicity and, thus, contributes to a more stable interaction between Ala138 (C-HR) and Leu45 (N-HR) through hydrophobic contacts.[12] In order to confirm the above hypothesis, the binding energies of C34 and $C34_{S138A}$ for the formation of the six-helix bundle were calculated using the X-ray coordinates.

Theoretical calculation of the binding free energies of C-HR-derived peptides

The single-point energy calculations with the FF99 force field were carried out to estimate the effects of the S138A substitution on the formation of the N-HR/C-HR six-helix bundle complex.

Figure 4a shows the intermolecular van der Waals interactions (ΔG_{vdW}) of each residue of C34 and $C34_{S138A}$ monomers in the complexes, which consist of the six-helix bundles formed with N36. The N-HR/C-HR interfacial residues (mainly *a* and *d* positions of the C-HR) of C34 and $C34_{S138A}$ interact strongly within the six-helix bundles. Besides the residues located at the N-HR/C-HR binding

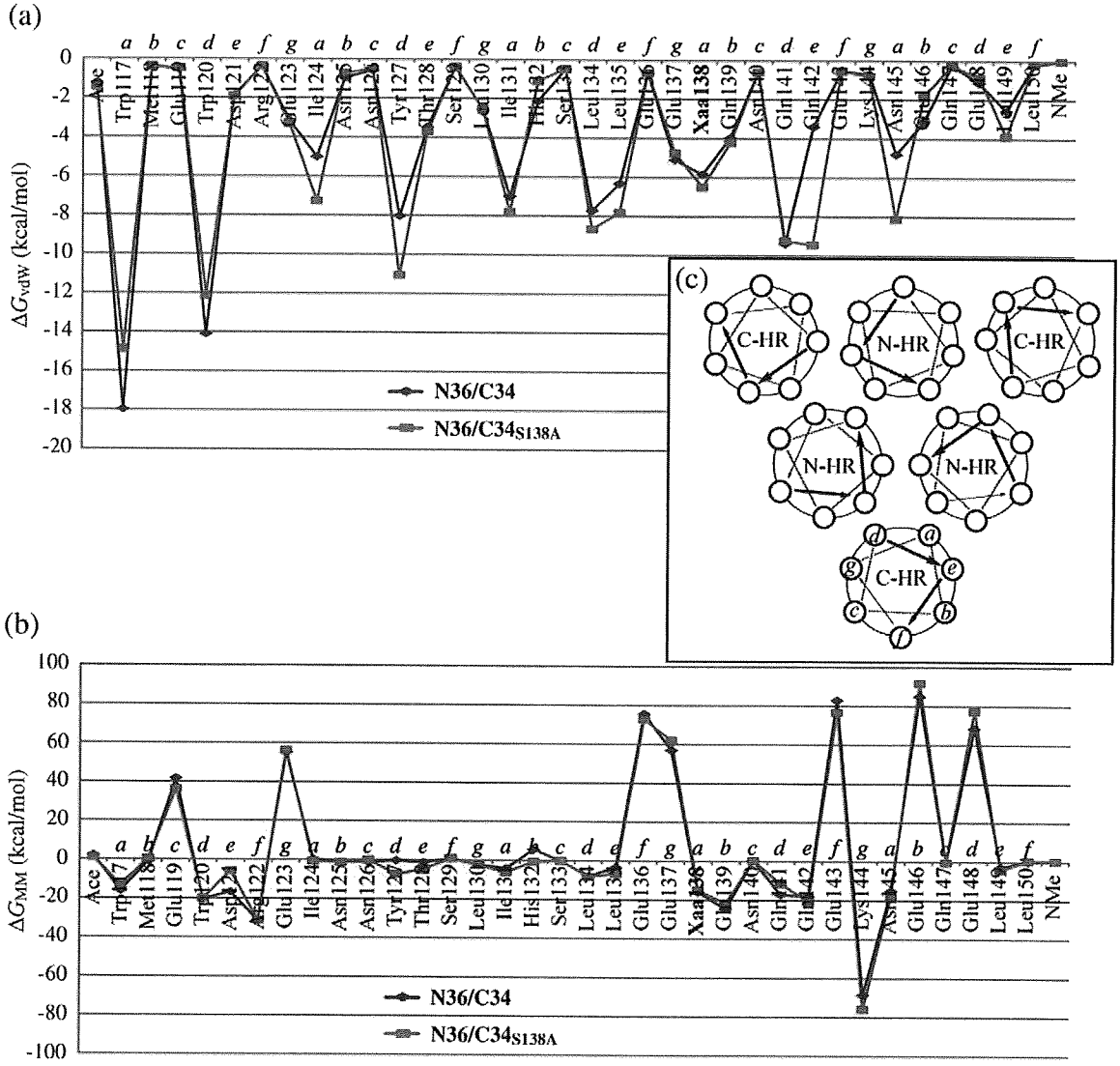

Fig. 4. Intermolecular interactions of each residue of the C-HR-derived peptides in the six-helix bundles: (a) the van der Waals interaction term (ΔG_{vdW}); (b) the pair interaction term (ΔG_{MM}), which combines the van der Waals and electrostatic interactions ($\Delta G_{vdW} + \Delta G_{ele}$); (c) helical-wheel representation of N-HR/C-HR six-helix bundle. The assignments of the residues are presented above the amino acid sequence by the italicized letters. Blue and red lines designate the interactions of C34 and $C34_{S138A}$, respectively.

interface, no significant differences between the ΔG_{vdW} values of each residue of C34 and $C34_{S138A}$ peptides were observed. ΔG_{vdW} of Gln142 located at the *e* position of the C-HR (near the substituted *a* position) was strongly enhanced by the S138A substitution. As shown in Table 3, the ΔG_{vdW} value of the $C34_{S138A}$ monomer was stabilized by 12 kcal/mol relative to the C34 monomer in the six-helix bundle (C34, $\Delta G_{vdW} = -126.76$ kcal/mol; $C34_{S138A}$, $\Delta G_{vdW} = -138.96$ kcal/mol). This indicated that the S138A substitution led to an improvement of the steric interactions between the N- and C-HRs.

Figure 4b shows the intermolecular pair interactions (ΔG_{MM}) of each residue of the C34 and $C34_{S138A}$ monomers in the six-helix bundles. Here, ΔG_{MM} was defined as a sum of the intermolecular van der Waals and electrostatic interactions ($\Delta G_{vdW} + \Delta G_{ele}$) serving to stabilize the six-helix bundle structures. The ΔG_{MM} values of all Glu residues (Glu119, Glu123, Glu136, Glu137, Glu143, Glu146, and Glu148) of C34 and $C34_{S138A}$ were estimated as large repulsive contributions. Accordingly, as shown in Table 3, the ΔG_{MM} of C34 and $C34_{S138A}$ monomers in the six-helix bundle structures gave rise to repulsive values (C34, $\Delta G_{MM} = 204.36$ kcal/mol; $C34_{S138A}$, $\Delta G_{MM} = 198.98$ kcal/mol). The repulsive ΔG_{MM} values arise because of the charge–charge repulsion between $C34_{S138X}$ (X=S or A) monomers and the N36/$C34_{S138X}$ (X=S or A) pentamers in the six-helix bundles [N36, +2 charge; C34 and $C34_{S138A}$, −6 charge; N36/C34 and N36/$C34_{S138A}$ pentamers, −6 charge (under standard ionization conditions)]. The Glu119, Glu136, and Glu143 residues (*c* and *f* positions of the C-HR) with small ΔG_{vdW} values were located at the solvent-accessible sites of the six-helix bundles and presumably interact with other species such as solvents or counterions to stabilize the six-helix bundle structures. To account for solvent effects, we applied MM and PBSA[20] methods to calculate the binding free energies (ΔG_{bind}) of C34 and $C34_{S138A}$ (Table 3). Here, ΔG_{bind} was defined as a sum of the intermolecular pair interactions and the desolvation free energies ($\Delta G_{MM} + \Delta G_{solv}$), serving to form the six-helix bundle complexes. The ΔG_{bind} values of C34 and $C34_{S138A}$ were −52.28 and −76.97 kcal/mol, respectively, and showed that both N36/C34 and N36/$C34_{S138A}$ complexes were stable despite the repulsive ΔG_{MM} values. Additionally, the G_{bind} of $C34_{S138A}$ was enhanced by 25 kcal/mol relative to that of C34. The ΔG_{bind} difference arises mainly from the desolvation free energy (ΔG_{solv}) of the $C34_{S138A}$ peptide being larger than the same energy for the C34 peptide (C34, $\Delta G_{solv} = -256.64$ kcal/mol; $C34_{S138A}$, $\Delta G_{solv} = -275.95$ kcal/mol). It seems that the ΔG_{solv} difference directly depends on the hydrophobicity of the substituted residue 138.

Table 3. Results of free-energy calculation by MM and PBSA

Peptides	ΔG_{MM}	ΔG_{vdW}	ΔG_{ele}	ΔG_{solv}	ΔG_{bind}
C34	204.36	−126.76	331.12	−256.64	−52.28
$C34_{S138A}$	198.98	−138.96	337.94	−275.95	−76.97
$C34_{S138A}$ simulation	209.56	−124.99	334.55	−264.94	−55.38

All energy values are given in kilocalories per mole. Peptides were capped with standard Ac and *N*-methylamide groups.

According to the crystal structure comparison between the wild-type and S138A mutant, the structural changes were extremely minor. Thus, we confirmed whether the effects of S138A substitution were predictable by simulation from the wild-type structure after removing the Ser138 oxygen atom. In both the X-ray and simulated structures of the S138A mutant, ΔG_{bind} was enhanced due to the increase in ΔG_{solv}. However, the simulated ΔG_{MM} and ΔG_{vdW} were weakened in contrast with those calculated from the X-ray structure, which was attributable to the different coordinates between the X-ray and simulated structures. This leads to different conclusions about the energy contributions of the S138A substitution and suggests that it is difficult to accurately estimate the mutation effects by simulation from the wild-type X-ray structure.

In order to consider the calculation errors, we performed the free-energy calculations against the candidate structures relaxed by using MM minimization with heavy atoms' positional constraints (Supplementary Data). When the heavy atoms were restrained with force constant 1000 kcal/(mol·Å^2), both the wild-type and S138A mutant structures were optimized with the all-heavy-atom RMSD of 0.01 Å, and these free-energy calculation errors were approximately 1 kcal/mol. Decreasing the force constant by 60 kcal/(mol·Å^2), both structures were optimized with the all-heavy-atom RMSD of 0.05 Å, and the calculation errors with respect to their ΔG_{MM} values were approximately 10 kcal/mol. Thus, the ΔG_{MM} values, which strongly depend on the atomic coordinates, may be inappropriate to understand the energy contributions to the stabilization of the six-helix bundles. On the other hand, the ΔG_{solv} values provided consistent and reliable results for the S138A substitution effects. As such, we concluded that the S138A substitution enhanced the ΔG_{bind} of the C-HR-derived peptide due to the increase in ΔG_{solv}.

We further investigated the ΔG_{vdW} and ΔG_{MM} of residue 138 in the six-helix bundles (Supplementary Data). As shown in Fig. 5, the S138A substitution increased ΔG_{MM} (ΔG_{vdW}) with Leu45. As such, the crystal-structure-based hypothesis that the S138A substitution led to a stable interaction between Ala138 (C-HR) and Leu45 (N-HR) was verified. Interestingly, the difference between the ΔG_{MM} of Ser138 and Ala138 with Leu45 was 2 kcal/mol and would have very little influence on the anti-HIV-1 activity of the C-HR-derived peptide because of the significantly larger ΔG_{solv} difference (25 kcal/mol).

These differences may also be positively involved in viral fusion. Since replication kinetics of variants that have mutations in the N-HR are generally impaired,[24] secondary mutations for efficiently

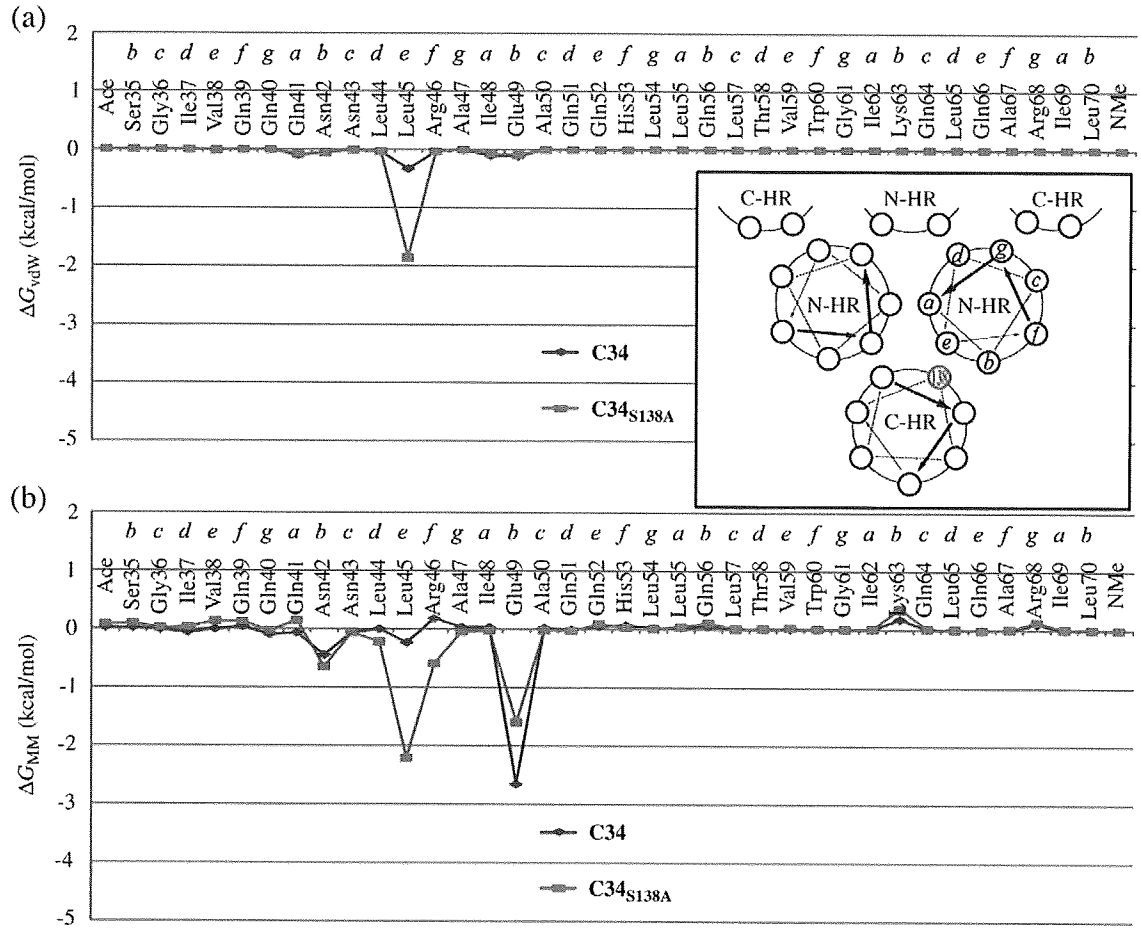

Fig. 5. Intermolecular interactions between residue 138 of the C-HR-derived peptides and one of the N-HR helices: (a) the van der Waals interaction term (ΔG_{vdW}); (b) the pair interaction term (ΔG_{MM}), which combines the van der Waals and electrostatic interactions ($\Delta G_{vdW} + \Delta G_{ele}$). Blue and red lines designate the interactions of C34 and $C34_{S138A}$, respectively. The assignments of the residues are presented above the amino acid sequence by the italicized letters.

replication may be required.[12,25] In this regard, we previously demonstrated that S138A acts as a secondary mutation and restores impaired replication kinetics by a primary mutation for T-20-resistant N43D.[19] Taken together, our observations are useful not only for the development of new peptidic and small molecular fusion inhibitors but also for the analysis of molecular mechanism of viral fusion.

Conclusion

We performed X-ray crystallographic analysis to evaluate the effects of the S138A substitution on the anti-HIV-1 activity of the C-HR-derived peptide C34. MM and PBSA calculations based on the X-ray coordinates were qualitatively supported by the difference between the experimental binding energies of the native and mutant C34 monomers. The N36/$C34_{S138A}$ complex was thermally more stable than the N36/C34 complex, and this result indicated that the S138A substitution accelerated the formation of the N-HR/C-HR six-helix bundle complex. This stability was found to be mainly caused by the difference between the desolvation energies of the C34 monomers with and without the S138A substitution. The desolvation energies depended on the hydrophobicity of residue 138. Therefore, the substitution of Ser138 to hydrophobic amino acids should enhance the anti-HIV-1 activities of the C-HR-derived peptides C34 and T-20.[19]

The crystal structure comparison between N36/C34 and N36/$C34_{S138A}$ complexes provided insights into the effect of S138A substitution on the binding affinities related with the anti-HIV-1 activities. We investigated whether the effects of the S138A substitution were predictable from the wild-type structure. The MM calculation of the wild-type X-ray structure after removing the Ser138 oxygen atom led to a different conclusion from that of the S138A X-ray structure. This result highlights the importance of atomic-level structure determination and indicates that the structural modeling of mutants starting from the wild-type X-ray structure should be carried out carefully. More reliable thermodynamic integration simulations are currently under investigation in order to predict the substitution effects *in silico*.

Materials and Methods

Peptide synthesis and purification

All peptides with an acetylated N-terminus and a C-terminal amide were synthesized by standard Fmoc-based peptide synthesis protocol using NovaSyn TGR resin. Fmoc amino acids had the following side-chain protections: *t*-butyl ester for Asp and Glu; trityl for His, Asn, and Gln; *t*-butyloxycarbonyl for Lys; 2,2,4,6,7-pentamethyldihydrobenzofuran-5-sulfonyl for Arg; *t*-butyl ether for Ser, Thr, and Tyr. The Fmoc amino acids were coupled, employing *N*,*N*′-diisopropylcarbodiimide in the presence of 1-hydroxybenzotriazole hydrate. After final deprotection and cleavage from the resins using a trifluoroacetic acid/thioanisole/*m*-cresol/1,2-ethanedithiol/water (80:5:5:5:5) cocktail, the crude peptides were purified by reverse-phase HPLC to yield the desired peptides, which were characterized by mass spectrometry (Supplementary Data).

Determination of drug susceptibility of HIV-1

The peptide sensitivity of infectious clones was determined by the MAGI assay with HeLa-CD4-LTR-β-gal cells and NL4-3(GIV) strain. The activity of test compounds was determined as the concentration that blocked HIV-1 replication by 50% (EC_{50}).[19,24]

Measurement of T_m value

Each peptide (10 μM) was mixed with 5 mM Hepes buffer (pH 7.2). CD spectra were acquired on a Jasco spectropolarimeter (Model J-710, Jasco Inc., Tokyo, Japan). The thermal stability was assessed by monitoring the change in the CD signal at 222 nm. The middle point of the thermal unfolding transition [melting temperature (T_m)] of each complex was determined (Supplementary Data).

Crystallization and X-ray analysis

Crystallization attempts were made using Hampton Crystal Screens I and II. Trials were performed by the sitting-drop vapor-diffusion method at 293 K. The drop contained 1 μL solution of the N36/$C34_{S138A}$ complex (2 mg/mL in 100 mM AcOH/Na, pH 4.0) and an equal volume of reservoir solution. To grow crystals, we diluted (1:1) a 2-mg/mL stock of the complex in a sitting drop with 12% ethanol and 400 mM magnesium chloride. The obtained crystal was transferred into a cryoprotectant consisting of 12% ethanol, 400 mM magnesium chloride, and 30% polyethylene glycol 400. Several minutes later, it was scooped up in a cryoloop and frozen in liquid nitrogen. It was then mounted on a goniometer in a nitrogen stream at 113 K. X-ray diffraction was detected on an R-AXIS VII imaging-plate system attached to a Rigaku CuKα radiation rotating-anode generator (FR-E) with a crystal-to-detector distance of 120 mm. Data were collected to 2.2 Å resolution (0.5 frames) with an exposure time of 2 min. The diffraction data were processed and scaled with d*TREK.[26] The N36/$C34_{S138A}$ complex structure was built by a molecular replacement calculation with the program MOLREP,[27] using the deposited coordinates of the N36/C34 complex (PDB code: 1AIK). Subsequent manual rebuilding was carried out in the program Coot.[28] The structure was refined by using the CCP4 program Refmac5.[29,30]

Computational methods

The heavy-atom coordinates of six-helix bundles (hexamers) of the peptide complexes (N36/C34 and N36/$C34_{S138A}$) were constructed on the basis of the X-ray crystal structures. By using the MOE software package,[31] the C-termini of the peptides were capped as *N*-methylamide group, and hydrogen atoms of the whole structures were placed at ideal positions. Subsequently, the energy minimizations were performed with the FF99 force field.[32] During the minimizations, all heavy atoms were fixed to the X-ray coordinates or restrained using force constants of between 0 and 10,000 kcal/(mol·Å^2). Then, the peptides were assumed as under a standard ionization condition.

Based on the resulting coordinates, the peptide–peptide pair interaction energies (ΔG_{MM}) were calculated by using the AMBER9 software package with the FF99 force field.[32,33] The solvation energies (ΔG_{solv}) were estimated by using the DELPHI program with PARSE radii,[20,34] AMBER partial charges, and dielectric constants of 1 (polypeptide interior) and 80 (water). The solvent-accessible surface areas were calculated using the MSMS program.[35] The desolvation energies (ΔG_{solv}) were defined as $\Delta G_{solv} = G_{solv}(\text{hexamer}) - G_{solv}(\text{pentamer}) - G_{solv}(\text{monomer})$. ΔG_{bind}, defined as a sum of the interaction energy (ΔG_{MM}) and the desolvation free energy (ΔG_{solv}), was obtained from $\Delta G_{bind} = G_{bind}(\text{hexamer}) - G_{bind}(\text{pentamer}) - G_{bind}(\text{monomer})$.

Accession code

Refined structure has been deposited in the PDB (PDB code: 2ZZO).

Acknowledgements

This work was supported by the Science and Technology Incubation Program in Advanced Regions from Japan Science and Technology Agency; a Grant-in-Aid for Scientific Research from the Ministry of Education, Culture, Sports, Science, and Technology of Japan; and Health and Labour Sciences Research Grants (Research on HIV/AIDS).

Supplementary Data

Supplementary data associated with this article can be found, in the online version, at doi:10.1016/j.jmb.2009.07.027

References

1. Lu, M., Blacklow, S. C. & Kim, P. S. (1995). A trimeric structural domain of the HIV-1 transmembrane glycoprotein. *Nat. Struct. Biol.* **2**, 1075–1082.

2. Chan, D. C., Fass, D., Berger, J. M. & Kim, P. S. (1997). Core structure of gp41 from the HIV envelope glycoprotein. *Cell*, **89**, 263–273.
3. Weissenhorn, W., Dessen, A., Harrison, S. C., Skehel, J. J. & Wiley, D. C. (1997). Atomic structure of the ectodomain from HIV-1 gp41. *Nature*, **387**, 426–430.
4. Melikyan, G. B., Markosyan, R. M., Hemmati, H., Delmedico, M. K., Lambert, D. M. & Cohen, F. S. (2000). Evidence that the transition of HIV-1 gp41 into a six-helix bundle, not the bundle configuration, induces membrane fusion. *J. Cell Biol.* **151**, 413–423.
5. Wild, C., Oas, T., McDanal, C., Bolognesi, D. & Matthews, T. (1992). A synthetic peptide inhibitor of human immunodeficiency virus replication: correlation between solution structure and viral inhibition. *Proc. Natl Acad. Sci. USA*, **89**, 10537–10541.
6. Wild, C. T., Shugars, D. C., Greenwell, T. K., McDanal, C. B. & Matthews, T. J. (1994). Peptides corresponding to a predictive alpha-helical domain of human immunodeficiency virus type 1 gp41 are potent inhibitors of virus infection. *Proc. Natl Acad. Sci. USA*, **91**, 9770–9774.
7. Chen, C. H., Matthews, T. J., McDanal, C. B., Bolognesi, D. P. & Greenberg, M. L. (1995). A molecular clasp in the human immunodeficiency virus (HIV) type 1 TM protein determines the anti-HIV activity of gp41 derivatives: implication of viral fusion. *J. Virol.* **69**, 3771–3777.
8. Kilby, J. M., Hopkins, S., Venetta, T. M., DiMassimo, B., Cloud, G. A., Lee, J. Y. *et al.* (1998). Potent suppression of HIV-1 replication in humans by T-20, a peptide inhibitor of gp41-mediated virus entry. *Nat. Med.* **4**, 1302–1307.
9. Matthews, T., Salgo, M., Greenberg, M., Chung, J., DeMasi, R. & Bolognesi, D. (2004). Enfuvirtide: the first therapy to inhibit the entry of HIV-1 into host CD4 lymphocytes. *Nat. Rev., Drug Discov.* **3**, 215–225.
10. Wei, X., Decker, J. M., Liu, H., Zhang, Z., Arani, R. B., Kilby, J. M. *et al.* (2002). Emergence of resistant human immunodeficiency virus type 1 in patients receiving fusion inhibitor (T-20) monotherapy. *Antimicrob. Agents Chemother.* **46**, 1896–1905.
11. Marcelin, A. G., Reynes, J., Yerly, S., Ktorza, N., Segondy, M., Piot, J. C. *et al.* (2004). Characterization of genotypic determinants in HR-1 and HR-2 gp41 domains in individual with persistent HIV viraemia under T-20. *AIDS*, **18**, 1340–1342.
12. Xu, L., Pozniak, A., Wildfire, A., Stanfield-Oakley, S. A., Mosier, S. M., Ratcliffe, D. *et al.* (2005). Emergence and evolution of enfuvirtide resistance following long-term therapy involves heptad repeat 2 mutations within gp41. *Antimicrob. Agents Chemother.* **49**, 1113–1119.
13. Otaka, A., Nakamura, M., Nameki, D., Kodama, E., Uchiyama, S., Nakamura, S. *et al.* (2002). Remodeling gp41-C34 peptide leads to high effective inhibitors of the fusion of HIV-1 with target cells. *Angew. Chem., Int. Ed.* **41**, 2937–2940.
14. Oishi, S., Ito, S., Nishikawa, H., Watanabe, K., Tanaka, M., Ohno, H. *et al.* (2008). Design of a novel HIV-1 fusion inhibitor that displays a minimal interface for binding affinity. *J. Med. Chem.* **51**, 388–391.
15. Joyce, J. G., Hunri, W. M., Bogusky, M. J., Garsky, V. M., Liang, X., Citron, M. P. *et al.* (2002). Enhancement of α-helicity in the HIV-1 inhibitory peptide DP178 leads to an increased affinity for human monoclonal antibody 2F5 but does not elicit neutralizing responses in vitro. *J. Biol. Chem.* **277**, 45811–45820.
16. Dweyr, J. J., Wilson, K. L., Davison, D. K., Freel, S. A., Seedolff, J. E., Wring, S. A. *et al.* (2007). Design of helical, oligomeric HIV-1 fusion inhibitor peptides with potent activity against enfuvirtide-resistant virus. *Proc. Natl Acad. Sci. USA*, **104**, 12772–12777.
17. Chan, D. C., Chutkowski, C. T. & Kim, P. S. (1998). Evidence that a prominent cavity in the coiled coil of HIV type 1 gp41 is an attractive drug target. *Proc. Natl Acad. Sci. USA*, **95**, 15613–15617.
18. Strockbine, B. & Rizzo, R. C. (2007). Binding of antifusion peptides with HIVgp41 from molecular dynamics simulations: quantitative correlation with experiment. *Proteins: Struct. Funct. Bioinform.* **67**, 630–642.
19. Izumi, K., Kodama, E., Shimura, K., Sakagami, Y., Watanabe, K., Ito, S. *et al.* (2009). Design of peptide-based inhibitors for human immunodeficiency virus type 1 strains resistant to T-20. *J. Biol. Chem.* **284**, 4914–4920.
20. Sitkoff, D., Sharp, K. A. & Honig, B. (1994). Accurate calculation of hydration free energies using macroscopic solvent models. *J. Phys. Chem.* **98**, 1978–1988.
21. Adachi, A., Gendelman, H. E., Koenig, S., Folks, T., Willey, R., Rabson, A. & Martin, M. A. (1986). Production of acquired immunodeficiency syndrome-associated retrovirus in human and nonhuman cells transfected with an infectious molecular clone. *J. Virol.* **59**, 284–291.
22. Judice, J. K., Tom, J. Y., Huang, W., Wrin, T., Vennari, J., Petropoulos, C. J. & McDowell, R. S. (1997). Inhibition of HIV type 1 infectivity by constrained α-helical peptides: implications for the viral fusion mechanism. *Proc. Natl Acad. Sci. USA*, **94**, 13426–13430.
23. Shu, W., Liu, J., Ji, H., Radigen, L., Jiang, S. & Lu, M. (2000). Helical interactions in the HIV-1 gp41 core reveal structural basis for the inhibitory activity of gp41 peptides. *Biochemistry*, **39**, 1634–1642.
24. Ueno, M., Kodama, E., Shimura, K., Sakurai, Y., Kajiwara, K., Sakagami, Y. *et al.* (2009). Synonymous mutations in stem–loop III of Rev responsive elements enhance HIV-1 replication impaired by primary mutations for resistance to enfuvirtide. *Antiviral Res.* **82**, 67–72.
25. Bai, X., Wilson, K. L., Seedorff, J. E., Ahrens, D., Green, J., Davison, D. K. *et al.* (2008). Impact of the enfuvirtide resistance mutation N43D and the associated baseline polymorphism E137K on peptide sensitivity and six-helix bundle structure. *Biochemistry*, **47**, 6662–6670.
26. Pflugrath, J. W. (1999). The finer things in X-ray diffraction data collection. *Acta Crystallogr., Sect. D: Biol. Crystallogr.* **55**, 1718–1725.
27. Vagin, A. & Teplyakov, A. (2000). An approach to multi-copy search in molecular replacement. *Acta Crystallogr., Sect. D: Biol. Crystallogr.* **56**, 1622–1624.
28. Emsley, P. & Cowtan, K. (2004). Coot: model-building tools for molecular graphics. *Acta Crystallogr., Sect. D: Biol. Crystallogr.* **60**, 2126–2132.
29. Collaborative Computational Project, Number 4. (1994). The CCP4 suite: programs for protein crystallography. *Acta Crystallogr., Sect. D: Biol. Crystallogr.* **50**, 760–763.
30. Murshudov, G. N., Vagin, A. A. & Dodson, E. J. (1997). Refinement of macromolecular structures by the maximum-likelihood method. *Acta Crystallogr., Sect. D: Biol. Crystallogr.* **53**, 240–255.
31. MOE software package from Chemical Computing Group Inc., http://www.chemcomp.com.
32. Wang, J. M., Cieplak, P. & Kollman, P. A. (2000). How well does a restrained electrostatic potential (RESP)

model perform in calculating conformational energies of organic and biological molecules. *J. Comput. Chem.* **21**, 1049–1074.

33. Pearlman, D. A., Case, D. A., Caldwell, J. W., Ross, W. R., Cheatham, T. E., DeBolt, S. *et al.* (1995). AMBER, a computer program for applying molecular mechanics, normal mode analysis, molecular dynamics and free energy calculations to elucidate the structures and energies of molecules. *Comp. Phys. Commun.* **91**, 1–41.
34. Honig, B. & Nicholls, A. (1995). Classical electrostatics in biology and chemistry. *Science*, **268**, 1144–1149.
35. Sanner, M. F., Olson, A. J. & Spehner, J. (1996). Reduced surface: an efficient way to compute molecular surfaces. *Biopolymers*, **38**, 305–320.

Bioorganic & Medicinal Chemistry 17 (2009) 7487–7492

Contents lists available at ScienceDirect

Bioorganic & Medicinal Chemistry

journal homepage: www.elsevier.com/locate/bmc

Bioorganic synthesis of end-capped anti-HIV peptides by simultaneous cyanocysteine-mediated cleavages of recombinant proteins

Michinori Tanaka [a], Kazumi Kajiwara [a,b], Rei Tokiwa [a,b], Kentaro Watanabe [a], Hiroaki Ohno [a], Hiroko Tsutsumi [c], Yoji Hata [c], Kazuki Izumi [d], Eiichi Kodama [d], Masao Matsuoka [d], Shinya Oishi [a,*], Nobutaka Fujii [a,*]

[a] Graduate School of Pharmaceutical Sciences, Kyoto University, Sakyo-ku, Kyoto 606-8501, Japan
[b] JST Innovation Plaza Kyoto, Japan Science and Technology Agency, Nishigyo-ku, Kyoto 615-8245, Japan
[c] Gekkeikan Research Institute, Gekkeikan Sake Company, Ltd, Fushimi-ku, Kyoto 612-8391, Japan
[d] Institute for Virus Research, Kyoto University, Sakyo-ku, Kyoto 606-8507, Japan

ARTICLE INFO

Article history:
Received 12 August 2009
Revised 5 September 2009
Accepted 10 September 2009
Available online 15 September 2009

Keywords:
Bioorganic synthesis
End-capped peptide
Fusion inhibitor
HIV-1

ABSTRACT

Bioorganic synthesis of N- and C-terminal end-capped peptides by two simultaneous *S*-cyanocysteine-mediated cleavages of recombinant proteins is described. This approach is demonstrated in the preparation of anti-HIV fusion inhibitory peptides.

1. Introduction

The recent upsurge of successes in recombinant protein-based therapeutics, such as antibodies and cytokines, as well as advances in formulation technology, has rekindled an interest in the potential development of biomolecule-derived pharmaceuticals such as peptides and oligonucleotides.[1] In order to accommodate large-scale production for high daily dose requirements, facile access to prepare homogeneous polymeric compounds is needed.[2] Expression by recombinant technology is an alternative to chemical synthesis of bioactive peptides. This approach can overcome major drawbacks associated with chemical synthesis including concomitant production of chemical wastes derived from protecting groups, organic solvents and resin for solid-phase synthesis. Conversely, recombinant peptides from prokaryotes are usually produced without post-translational modifications. Such modifications often provide characteristic functions including bioactivity and biostability.[3,4]

Proteolytic cleavage by exopeptidases is one of the main pathways for degradation of bioactive peptides under physiological conditions. In order to maintain the prolonged effect of peptide therapeutics in vivo, the design of N-terminal acyl- and/or C-terminal amide-modified peptides has been attempted. Such modifications can prevent enzymatic scissions in the circulatory system. However, practical recombinant methodology to prepare bioactive peptides having two end-capping groups is not established. Site-specific cleavage at the *S*-cyanocysteine site within recombinant proteins **2** in the presence of ammonia has been reported (Scheme 1).[5] Such a reaction gives rise to peptide acids and amides **4**. This reaction concomitantly releases the tail peptide **5** with a 2-iminothiazolidine-4-carbonyl group at the N-terminus. On the basis of this chemistry, we envisaged that cleavages of **6** at two *S*-cyanocysteines across the target peptide sequence would generate a peptide amide modification **7** with an N-terminal 2-iminothiazolidine-4-carbonyl group. The current work represents the facile preparation of N- and C-terminally protected anti-HIV peptides by two simultaneous chemical cleavages of recombinant proteins.

2. Results and discussion

This type of cleavage presumably consists of nucleophilic attack of amines and the consecutive iminothiazolidine formation (Scheme 1). Since β-elimination of the thiocyanato group is a possible competing reaction of *S*-cyanocysteine, rapid progression of

* Corresponding authors. Tel.: +81 75 753 4551; fax: +81 75 753 4570 (S.O.).
E-mail addresses: soishi@pharm.kyoto-u.ac.jp (S. Oishi), nfujii@pharm.kyoto-u.ac.jp (N. Fujii).

0968-0896/$ - see front matter © 2009 Elsevier Ltd. All rights reserved.
doi:10.1016/j.bmc.2009.09.015

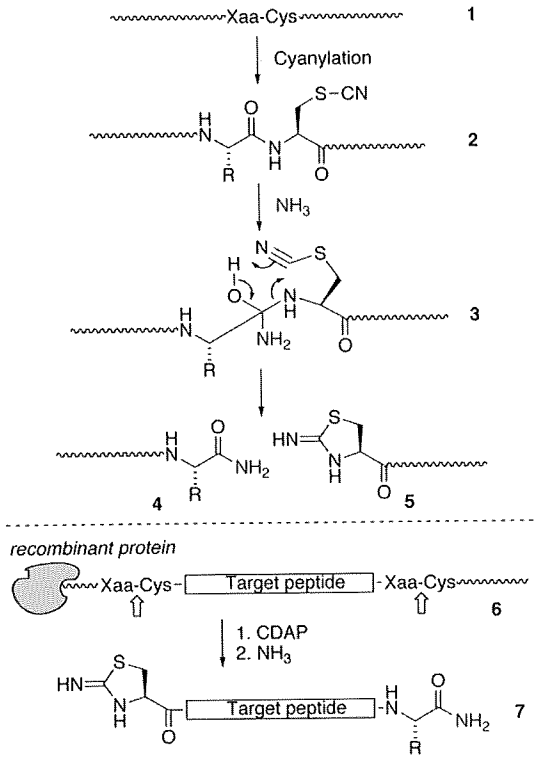

Scheme 1. Site-specific cleavage of recombinant proteins at *S*-cyanocysteine and the preparative illustration of N- and C-terminally capped peptide **7**.

these two steps is preferred.[6] We expected that the presence of an appropriate side-chain functional group in close proximity should assist the cleavage.[7] Using model synthetic peptides Ac-YEQQK-X-C-EEYFKK-NH_2 **8**, we evaluated the effect of the N-terminal-side residue (X) of the cysteine on peptide amide formation. After the standard Fmoc-based solid-phase peptide synthesis, the peptides **8** were treated with 1-cyano-4-dimethylaminopyridinium tetrafluoroborate (CDAP) in a 0.1 N AcOH solution to provide S-cyanylated peptides **9**, which were purified by RP-HPLC. Cleavage reactions of **9** with aqueous 3 M NH_3 were monitored by RP-HPLC analysis (Table 1), in which the production of the first segment peptides **10a,b** and the second segment **11** with the N-terminal 2-iminothiazolidine-4-carbonyl group were expected. Among the 19 natural amino acids utilized for the X position (except Cys), bulky aliphatic amino acids such as Val, Ile, and Pro were unfavorable for the cleavage reaction. Peptides with an acidic amino acid such as Asp and Glu mainly provided a β-eliminated product **12**.[8] In contrast, Ser and Thr were appropriate residues for the cleavage reaction. Interestingly, the reaction of Asn- and Lys-containing peptides accompanied production of characteristic C-terminally protected peptides **13** and **14** in higher combined yields: from the Asn peptide, formation of C-terminal aspartimide **13** was observed along with the C-terminal peptide amide (**10a**:**13** = 53:47).[9] Cleavage of the Lys peptide produced a peptide **14** with a C-terminal seven-membered lactam preferentially over the C-terminal amide form (**10a**:**14** = 22:78).[10]

C-terminal cyclic structures in aspartimide **13** and lactam **14** were verified by ESI LC/MS/MS and by the comparative analysis using the peptides that were prepared by the alternative procedures (Scheme 2). Briefly, (*S*)-3-aminosuccinimide **15a** or (*S*)-3-amino-ε-caprolactam **15b** was coupled with Fmoc-Lys(Boc)-OH to give the protected C-terminal components **16a,b**. After Boc-deprotection of **16a,b**, the resulting amine **17a,b** were anchored onto *p*-nitrophenyl carbonate resin, which was prepared by treatment of NovaSyn TGA resin with 4-nitrophenyl chroloformate.

Table 1
Cleavage reaction of *S*-cyanocysteine-containing peptides **9** by aqueous NH_3[a]

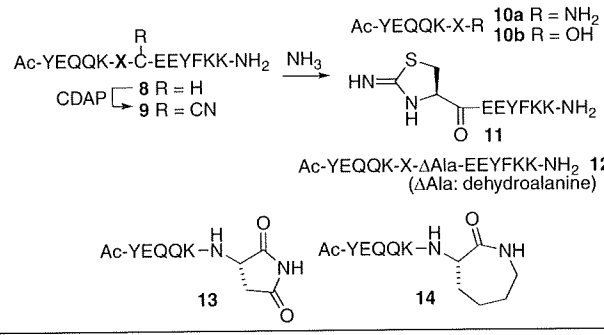

X	Conversion[b] (%)
Gly	50
Ala	62
Val	36
Leu	53
Ile	46
Pro	42
Met	66
Phe	63
Tyr	55
Trp	57
Ser	68
Thr	71
Asp	45
Glu	46
Asn	79[c]
Gln	65
Lys	82[d]
Arg	71
His	64

[a] All cleavage reactions were carried out in 3 M NH_3 for 20 min at 20 °C.
[b] The conversion yields were calculated based on the combined peak areas of peptides **10a** and **11** by RP-HPLC analysis.
[c] Including C-terminal aspartimide product **13** (**10a**:**13** = 53:47).
[d] Including C-terminal ε-lactam product **14** (**10a**:**14** = 22:78).

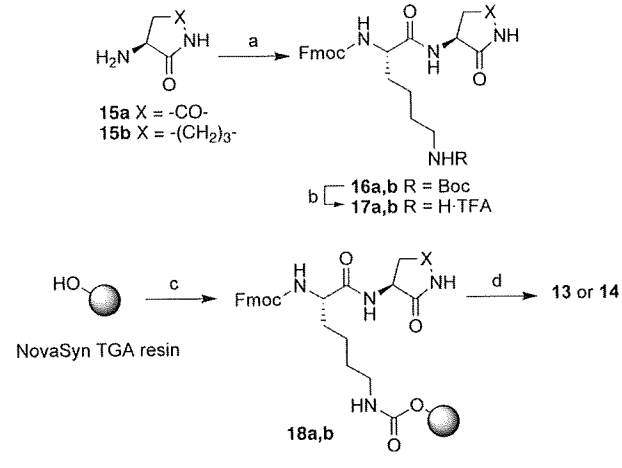

Scheme 2. Alternative synthesis of peptides **13** and **14**. Reagents and conditions: (a) Fmoc-Lys(Boc)-OH, HOBt·H_2O, WSC·HCl, (*S*)-3-aminosuccinimide for **16a** (94%) or (*S*)-3-amino-ε-caprolactam for **16b** (99%); (b) 95% aqueous TFA (quant.); (c) (i) 4-nitrophenyl chloroformate, (*i*-Pr)$_2$EtN, DCM; (ii) **17a** or **17b**, (*i*-Pr)$_2$EtN, DMF (**18a**: 51% loading, **18b**: 45% loading); (d) (i) Fmoc-based SPPS; (ii) TFA/H_2O/*m*-cresol/thioanisole/1,2-ethanedithiol (80:5:5:5:5).

Fmoc-based solid-phase synthesis of the peptide sequence followed by final deprotection gave the expected peptides **13** and

14. Comparative RP-HPLC analysis demonstrated that the peptides were coincident with the ones obtained by cyanocysteine-mediated cleavage (see Supplementary data).

Both the ring structures of **13** and **14** were formed by intramolecular cyclization of characteristic side-chains of Asn and Lys under basic conditions. Since intramolecular imide or amide formation was expected to assist the rapid cleavage, we searched for appropriate conditions for two simultaneous ring-closing reactions including C-terminal aspartimide **13** or lysine ε-lactam **14** as well as N-terminal iminothiazolidine formations (Table 2). Tertiary amines such as Et_3N and $(i\text{-}Pr)_2EtN$ generated the expected two peptides **13** and **14** with cyclic structures. Treatment of **9** with alkaline metal-based weak bases such as $NaHCO_3$ and AcONa recovered the starting material, while the expected **13** or **14** was predominantly obtained by aqueous carbonates.[11] Aqueous 0.3 M K_2CO_3, which provided **13** or **14** most efficiently, was employed for further experiments.

The established protocol was applied to bioorganic synthesis of anti-HIV peptides from recombinant proteins. As a model peptide, HIV fusion inhibitor SC34EK **19** was utilized, which was designed based on the bioactive α-helix conformation of the C-terminal heptad repeat in the envelop glycoprotein gp41 (Table 3, Scheme 3).[12] Peptide **19** exerts anti-HIV activity by preventing formation of the fusogenic six-helical bundle of gp41 and is potent against wild-type and enfuvirtide-resistant HIV-1 viruses. The recombinant thioredoxin-fused proteins **22a,b** containing anti-HIV sequence were expressed using the *Escherichia coli* BL21 strain and were purified by affinity chromatography using Ni-NTA resin. After the removal of imidazole by gel filtration, the protein concentration was quantified by the standard Bradford assay. S-Cyanylation of **22a,b** was carried out with 10 mM CDAP in 0.1 N AcOH containing 0.5 mM tris(2-carboxyethyl)phosphine (TCEP), which was added to maintain reducing condition for keeping Cys residues.[6b,13] The resulting cyanylated proteins **23a,b** were treated in a K_2CO_3 solution (0.3 M) to provide the expected end-capped peptides **20a** and **20b** in 24% and 21% isolated yields, respectively (Fig. 1) and were accompanied with the thioredoxin parts **24a,b**.[14]

Anti-HIV activity of the peptides **20a,b** derived from recombinant proteins was evaluated along with the parent SC34EK **19** and the end-capping free **21**, which is usually expressed in prokaryotes (Table 3). Peptides **20a,b** reproduced the bioactivity of the original peptide **19** [EC_{50}(**20a**) = 0.48 nM; EC_{50}(**20b**) = 0.58 nM],[15] indicating that the original anti-HIV activity was not

Table 3
Sequences and anti-HIV activity of N- and C-terminally capped SC34EK analogs

Peptide	R^1-WMEWDRKIEEYTKKIEELIKKSQEQQEKNEKELK-R^2 **19–21** R^1	R^2	EC_{50}[a] (nM)	T_m (°C)
SC34EK **19**	Ac	NH_2	0.60 ± 0.10	71.2
20a	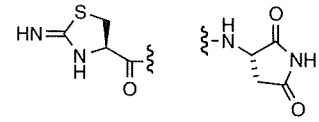		0.48 ± 0.13	71.0
20b	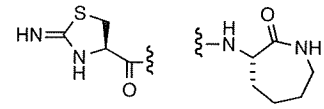		0.58 ± 0.24	71.0
21	H	OH	0.68 ± 0.11	—

[a] EC_{50} was determined as the concentration that blocked HIV-1 replication by 50% in a MAGI assay.

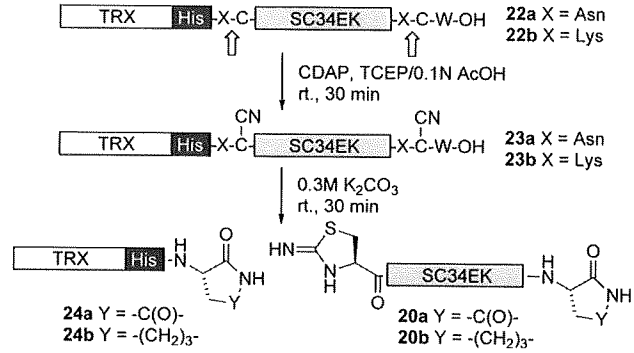

Scheme 3. Bioorganic synthesis of anti-HIV peptide SC34EK analogs **20a,b** including N- and C-terminal capping moieties.

Table 2
Cleavage reaction of Asn-Cys(CN) or Lys-Cys(CN)-containing peptides by basic treatment[a]

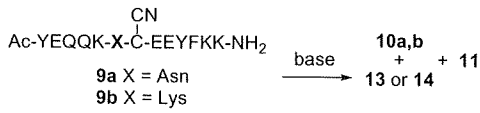

Entry	Base	From peptide **9a**		From peptide **9b**	
		Conversion[b] (%)	Ratio (**13**/**10**)[c]	Conversion[b] (%)	Ratio (**14**/**10**)[c]
1	3 M NH_3	79	0.9	82	3.6
2	0.5 M NH_3	59	1.7	72	12.4
3	1 M Et_3N	70	3.6	64	>30
4	1 M $(i\text{-}Pr)_2EtN$	63	3.1	65	>30
5	1 M AcONa	—[d]	—	—[d]	—
6	1 M $NaHCO_3$	—[d]	—	—[d]	—
7	1 M Na_2CO_3	85	2.5	64	5.6
8	0.3 M Na_2CO_3	83	3.3	74	13.5
9	1 M K_2CO_3	85	1.8	68	9.7
10	0.3 M K_2CO_3	83	3.5	73	15.6

[a] All cleavage reactions were carried out for 20 min at 20 °C.
[b] The conversion yields were calculated based on the combined peak areas of peptides **10a** (entries 1 and 2)/**10b** (entries 3–10), **11**, and **13** or **14** by RP-HPLC analysis.
[c] The ratios of the peak areas of aspartimide **13** or ε-lactam **14** to peptide **10**.
[d] The starting material was recovered.

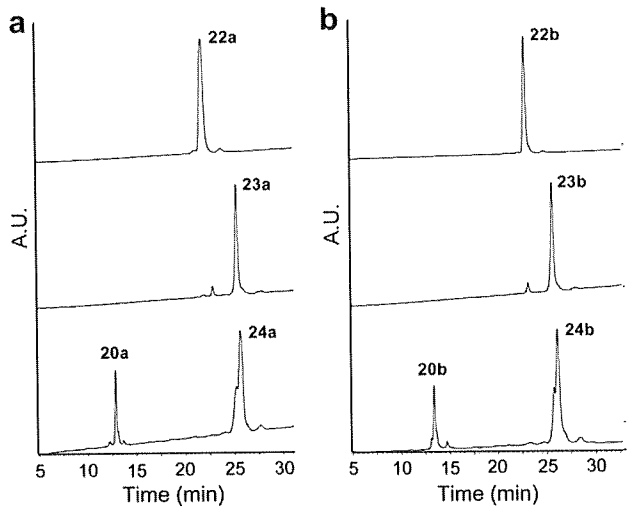

Figure 1. HPLC profiles of *S*-cyanocysteine-mediated cleavage of thioredoxin-fused proteins. (a) Asn-Cys(CN)-mediated cleavage; (b) Lys-Cys(CN)-mediated cleavage. Top: recombinant proteins **22a,b** purified by affinity chromatography; middle: *S*-cyanylated products **23a,b**; bottom: products from basic treatment of **23a,b**. *HPLC conditions*: linear gradient of 30–60% solvent B in solvent A over 30 min.

disturbed by the N- and C-terminal functional end-capping groups. Biophysical characterization of these peptides was investigated by circular dichroism (CD) analysis (Fig. 2 and Supplementary data). The improved α-helix property of **19** is retained in **20a** and **20b**, and similar thermal stability of the six-helical bundle with N36 was observed (Table 3).

The protecting ability of iminothiazolidine for the N-terminus as well as lysine ε-lactam and aspartimide for the C-terminus from the biodegradation by potential exopeptidases was assessed using peptides **19–21**. The quantity of the intact peptide during incubation in mouse serum was monitored by RP-HPLC (Fig. 3). Rapid degradation was observed for peptide without capping groups at both ends. The isolated digested product had two C-terminal residues deleted. Similarly, C-terminal aspartimide peptide **20a** was also gradually degraded at the C-terminus.[16] In contrast, peptide **20b** with a C-terminal ε-lactam was stable during the 24-h incubation. As such, a combination of iminothiazolidine at the N-terminus and lysine ε-lactam at the C-terminus is beneficial for stabilizing the anti-HIV peptide against potential exopeptidase-mediated degradation without alteration of the biological and biophysical characters.

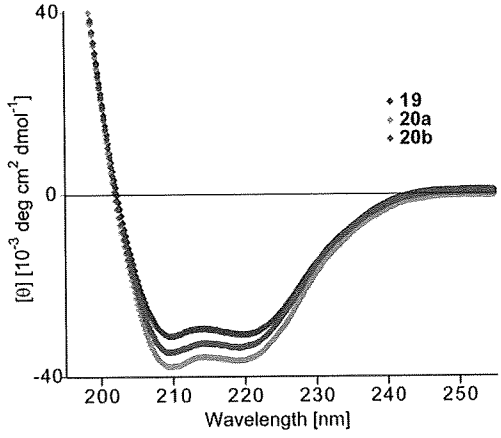

Figure 2. Circular dichroism spectra of N36-SC34EK analogue complexes.

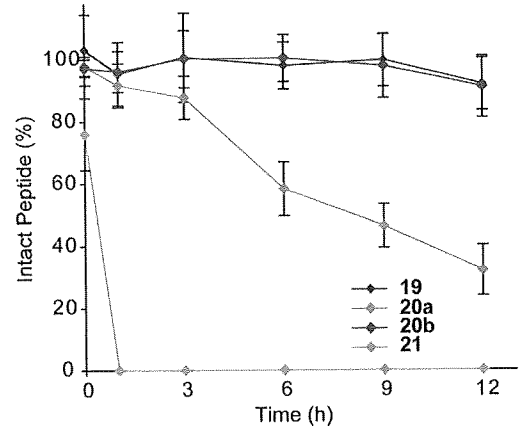

Figure 3. Degradation of SC34EK **19** and the analogues **20a,b**, **21** in mouse serum ($n = 5$).

3. Conclusions

Reported herein is the bioorganic synthesis of anti-HIV peptides with two end-capping groups from recombinant proteins. *S*-Cyanocysteine-mediated cleavage at the Asn-Cys(CN) and Lys-Cys(CN) sites provided the characteristic C-terminal ring structures, aspartimide and lysine ε-lactam, respectively. These ring structures are not found in recombinant proteins and peptides produced from prokaryotes. In the current anti-HIV peptide study, capping functional groups did not disturb the original potent bioactivity or modify the biophysical character. This approach is applicable to the preparation of plural end-capped peptides from a single protein molecule having tandem target sequences in conjunction with Lys-Cys(CN) sites.

4. Experimental

4.1. General

For HPLC separations of synthetic peptides, a Cosmosil 5C18-ARII analytical column (4.6 × 250 mm, flow rate 1 mL/min, Nacalai Tesque, Kyoto Japan) or a Cosmosil 5C18-ARII preparative column (20 × 250 mm, flow rate 10 mL/min) was employed. For HPLC analysis of recombinant proteins **22a,b**, **23a,b** and the cleaved products **20a,b** (Fig. 1), a Cosmosil Protein-R analytical column (4.6 × 150 mm, flow rate 1 mL/min) was employed. The eluting products were detected by UV at 220 nm. A solvent system consisting of 0.1% TFA solution (v/v, solvent A) and 0.1% TFA in MeCN (v/v, solvent B) were used for HPLC elution. All peptides were characterized by a MALDI-TOF-MS (AXIMA-CFR plus, Shimadzu, Kyoto, Japan) or by a QqTof (QSTAR pulsar i, Applied Biosystems). NMR spectra were recorded on Bruker AVANCE500.

4.2. Peptide synthesis

Protected peptide-resins were manually constructed by standard Fmoc-based SPPS on Rink Amide resin (Novabiochem, 83 mg, 0.05 mmol). *t*-Bu for Tyr, Ser and Thr; *t*-Bu ester for Asp and Glu; Boc for Lys; Trt for Cys, His, Asn and Gln; and 2,2,4,6,7-pentamethyldihydrobenzofuran-5-sulfonyl (Pbf) for Arg were employed for side-chain protection, respectively. Fmoc-amino acids were coupled using 5 equiv of reagents [Fmoc-amino acid, *N,N'*-diisopropylcarbodiimide and HOBt·H_2O] to free amino group in DMF for 1.5 h. Fmoc deprotection was performed by 20% piperidine in DMF (2 × 1 min, 1 × 20 min). The resulting protected resin was treated with TFA/H_2O/*m*-cresol/thioanisole/1,2-ethanedithiol

(80:5:5:5:5) at room temperature for 2 h. After removal of the resin by filtration, ice-cold dry Et_2O (30 mL) was added to the residue. The resulting powder was collected by centrifugation and then washed with ice-cold dry Et_2O (3 × 15 mL). Purification of the crude product by preparative HPLC afforded a colorless powder of the desired peptide.

4.3. General procedure for the preparation of *S*-cyanocysteine-containing peptides 9

To a solution of peptide **8** (X = Lys, 5.8 mg) in 0.1 N AcOH (0.58 mL) was added the solution of CDAP in 0.1 N AcOH (10 mg/mL, 182 μL). After being stirred at room temperature for 30 min, the solution was purified by preparative HPLC to give freeze-dried powder of peptide **9** (X = Lys, 5.7 mg, 97%).

4.4. General procedure for cleavage reaction of *S*-cyanocysteine-containing peptides 9 by aqueous NH_3

Peptide **9** (ca. 1 mg) was dissolved in 100 μL of 3 M NH_3 solution. After standing at 20 °C for 20 min, the reaction was monitored by RP-HPLC. The results are summarized in Table 1.

4.5. Synthesis of compound 16a

To a solution of Fmoc-Lys(Boc)-OH (2.34 g, 5.0 mmol) and HOBt·H_2O (0.77 g, 5.0 mmol) in DMF (20 mL) was added WSC·HCl (0.96 g, 5.0 mmol) at 0 °C. After being stirred for 5 min. at room temperature, a solution of (*S*)-3-aminosuccinimide **15a** [prepared by catalytic hydrogenation of (*S*)-3-*N*-carbobenzoxyaminosuccinimide (1.61 g, 6.5 mmol)] in DMF (5 mL) was added. The reaction mixture was stirred for 1 h and was poured into ice-cold water. The resulting precipitate was extracted with AcOEt and the organic layer was washed with citric acid solution and brine. After drying over $MgSO_4$, the solvent was evaporated under reduced pressure. The residue was purified by silica-gel column chromatography to provide the compound **16a** (2.65 g, 94% yield) as a colorless powder: $[\alpha]_D^{20}$ −31.4 (*c* 1.0, $CHCl_3$); ^1H NMR (500 MHz, DMSO-d_6) δ 11.22 (s, 1H), 8.51 (d, *J* = 8.0 Hz, 1H), 7.92–7.80 (m, 2H), 7.75–7.66 (m, 2H), 7.52 (d, *J* = 8.0 Hz, 1H), 7.44–7.36 (m, 2H), 7.36–7.27 (m, 2H), 6.78 (t, *J* = 5.5 Hz, 1H), 4.59–4.46 (m, 1H), 4.34–4.14 (m, 3H), 3.98–3.83 (m, 1H), 2.94–2.78 (m, 3H), 2.42 (dd, *J* = 17.5, 5.5 Hz, 1H), 1.69–1.43 (m, 2H), 1.42–1.11 (m, 13H). ^{13}C NMR (125 MHz, DMSO-d_6) δ 177.4, 176.3, 172.1, 155.9, 155.5, 143.8, 143.6, 140.6, 127.5, 127.0, 125.3, 120.0, 77.2, 65.6, 54.3, 49.2, 46.6, 38.9, 36.0, 31.4, 29.0, 28.2, 22.6. Anal. Calcd for $C_{30}H_{36}N_4O_7·H_2O$: C, 61.84; H, 6.57; N, 9.62. Found: C, 61.92; H, 6.23; N, 9.72.

4.6. Synthesis of compound 16b

To a solution of Fmoc-Lys(Boc)-OH (2.34 g, 5.0 mmol) and HOBt·H_2O (0.77 g, 5.0 mmol) in DMF (20 mL) was added WSC·HCl (0.96 g, 5.0 mmol) at 0 °C. After being stirred for 5 min at room temperature, a solution of (*S*)-3-amino-ε-caprolactam **15b** (0.77 g, 6.0 mmol) in DMF (5 mL) was added. The reaction mixture was stirred for 1 h, and was poured into ice-cold water. The resulting precipitate was extracted with AcOEt and the organic layer was washed with citric acid solution and brine. After drying over $MgSO_4$, the solvent was evaporated under reduced pressure. The residue was purified by silica-gel column chromatography to provide the compound **16b** (2.86 g, 99% yield) as a colorless powder: $[\alpha]_D^{20}$ −8.6 (c 1.0, $CDCl_3$); ^1H NMR (500 MHz, DMSO-d_6) δ 7.92–7.82 (m, 3H), 7.81 (d, *J* = 6.5 Hz, 1H), 7.76–7.69 (m, 2H), 7.67 (d, *J* = 8.0 Hz, 1H), 7.45–7.38 (m, 2H), 7.36–7.25 (m, 2H), 6.78 (t, *J* = 5.5 Hz, 1H), 4.40–4.30 (m, 1H), 4.30–4.13 (m, 3H), 4.00–3.89 (m, 1H), 3.23–3.14 (m, 1H), 3.10–3.00 (m, 1H), 2.96–2.81 (m, 2H), 1.90–1.80 (m, 1H), 1.80–1.69 (m, 2H), 1.69–1.56 (m, 2H), 1.56–1.46 (m, 1H), 1.42–1.12 (m, 15H); ^{13}C NMR (125 MHz, DMSO-d_6) δ 174.0, 170.8, 155.9, 155.5, 143.8, 143.6, 140.6, 127.5, 125.3, 125.2, 120.0, 77.2, 65.6, 54.9, 51.2, 46.6, 40.5, 31.3, 30.9, 29.1, 28.7, 28.2, 27.5, 22.8. Anal. Calcd for $C_{32}H_{42}N_4O_6$: C, 66.41; H, 7.32; N, 9.68. Found: C, 66.17; H, 7.03; N, 9.71.

4.7. Synthesis of resin 18a

Compound **16a** (0.56 g, 1 mmol) was dissolved in 95% aqueous TFA (5 ml) and the solution was stirred at room temperature for 1 h. The solvent was removed under reduced pressure to give compound **17a** (0.58 g, quant.) as a colorless oil, which was utilized for the next step without further purification. A solution of 0.3 M 4-nitrophenyl chloroformate and 0.3 M (*i*-Pr)$_2$EtN in DCM (2 mL) was added to NovaSyn TGA resin (0.26 mmol/g, 192 mg, 0.05 mmol). The mixture was stirred at room temperature for 4 h, and the resin was washed with DCM (×3) and DMF (×3). A solution of 0.3 M compound **17a**, 0.3 M (*i*-Pr)$_2$EtN in DMF (2 mL) was added to the resin and the mixture was stirred at room temperature for 6 h. The resin was washed by DMF (×5), DCM (×3) and MeOH (×3) and dried to give the expected resin **18a** (51% loading).

4.8. Preparation of recombinant thioredoxin-fused proteins 22a,b

The cDNA sequence encoding KKC-SC34EK-KCW and KNC-SC34EK-NCW was utilized as template for PCR amplification, KNC-SC34EK-NCW: 5′-CTC**GGATCC**AAAAATTGCTGGATGGAATGGG ATCGTAAAATTGAAGAATATACCAAAAAAATTGAAGAACTGATTAAAA AAAGCCAGGAACAGCAGGAAAAAAATGAAAAAGAACTGAAAAATTGC TGGTAA**CTCGAG**-3′; KKC-SC34EK-KCW: 5′-CTC**GGATCC**AAAAAATG CTGGATGGAATGGGATCGTAAAATTGAAGAATATACCAAAAAAATTGA AGAACTGATTAAAAAAAAGCCAGGAACAGCAGGAAAAAAATGAAAAA GAACTGAAAAAATGCTGGTAA**CTCGAG**GAG-3′. The two restriction sites for BamHI and XhoI are shown in bold. Codons were replaced by more frequently used ones based on *E. coli.* codon usage. Each segment was digested with BamHI and XhoI and inserted into pET32a vector. Then the plasmids (pET32a-KKC-SC34EK-KCW and pET32a-KNC-SC34EK-NCW) were transformed into *E. coli* BL21 (DE3)-RIL strain for expression. Isolated colonies were picked up and cultured overnight in 10 mL of LB culture with 50 μg/mL ampicillin at 30 °C with shaking. This culture was transferred into 1 L of LB culture in the presence of 50 μg/mL ampicillin. When the OD_{600} reached 0.6–0.8 at 30 °C, protein expression was initiated by adding isopropyl β-D-1-thiogalactopyranoside (IPTG) (1 mM). After an additional 6 h cultivation at 25 °C, cells were harvested by centrifugation at 4000 rpm for 20 min. Cells were resuspended in B-PER (PIERCE) solution, and disrupted by sonication. After centrifugation at 12,000 rpm for 30 min, the supernatant, supplemented 0.5 mM TCEP, was transferred to column with Ni-NTA agarose (QIAGEN). The column was washed with wash buffer (20 mM phosphate, pH 6.0, containing 0.5 M NaCl and 0.5 mM TCEP). Protein was eluted from the column by the 150 mM imidazole in phosphate buffer (pH 6.0) containing 0.5 mM TCEP. The expression and purification of the fusion protein was analyzed by SDS–PAGE (10–20% gradient gel). The yield of eluted protein was calculated using Protein Assay Kit (BIO-RAD).

4.9. General procedure for the preparation of the end-capped anti-HIV peptide from recombinant protein

The eluted protein **22a** (6.8 mg quantified by Bradford assay) from the NAP column (GE healthcare) was cyanylated by 10 mM CDAP in the 0.1 N AcOH containing 0.5 mM TCEP for 30 min. After

desalting by gel-filtration and freeze-drying, cyanylated protein was treated with 0.3 M K_2CO_3 for 30 min. The reaction products were analyzed using LC–MS. Purification of the product by preparative HPLC provided the expected end-capped peptide **20a** (0.40 mg, 24%) that was quantified by UV absorbance at 280 nm.

4.10. Determination of drug susceptibility of HIV-1

The peptide sensitivity of infectious clones was determined by the MAGI assay with some modifications.[17] Briefly, the target cells (HeLa-CD4-LTR-β-gal; 10^4 cells/well) were plated in 96-well flat microtiter culture plates. On the following day, the cells were inoculated with the HIV-1 clone (NL4-3, 60 MAGI U/well, giving 60 blue cells after 48 h of incubation) and cultured in the presence of various concentrations of drugs in fresh medium. Forty-eight hours after viral exposure, all the blue cells stained with X-Gal (5-bromo-4-chloro-3-indolyl-β-D-galactopyranoside) were counted in each well. The activity of test compounds was determined as the concentration that blocked HIV-1 replication by 50% (50% effective concentration [EC_{50}]).

4.11. Measurement of CD spectra

Peptides **19** and **20a,b** were incubated at 37 °C for 30 min (the final concentrations of peptides were 10 μM in 5 mM HEPES buffer, pH 7.2). CD spectra were acquired on a Jasco spectropolarimeter (Model J-710, Jasco Inc., Tokyo, Japan) at 25 °C as the average of 8 scans. Thermal unfolding of potential six-helical bundle in the presence of N36 was monitored by the $[\theta]_{222}$ values at intervals of 0.5 °C after a 0.25-min equilibration at the desired temperature and an integration time of 1.0 s. The midpoint of the thermal unfolding transition of each complex was defined as the melting temperature (T_m).

4.12. Stability of SC34EK peptide or analogs in mouse serum

Peptides **19-21** (0.5 mM in PBS) were incubated at 37 °C in 50% mouse serum in the presence of 0.1% *m*-cresol (internal standard). 0.010 mL samples were collected at 0, 1, 3, 6, 9 and 12 h and the reaction was terminated by the addition of 1 μL 0.1 N HCl and 0.040 mL of CH_3CN. Samples were deproteinized by centrifugation at 12000 rpm for 10 min and 0.010 mL of the supernatant was injected into LC-MS. The percentage of intact peptides was calculated by peak area and corrected against the internal standard.

Acknowledgments

This work was supported by Science and Technology Incubation Program in Advanced Regions from Japan Science and Technology Agency, Grants-in-Aid for Scientific Research from the Ministry of Education, Culture, Sports, Science, and Technology of Japan, and Health and Labour Sciences Research Grants (Research on HIV/AIDS).

Supplementary data

Supplementary data associated with this article can be found, in the online version, at doi:10.1016/j.bmc.2009.09.015.

References and notes

1. For reviews, see: (a) Frokjaer, S.; Otzen, D. E. *Nat. Rev. Drug Disc.* **2005**, *4*, 298; (b) Leader, B.; Baca, Q. J.; Golan, D. E. *Nat. Rev. Drug Disc.* **2008**, *7*, 21.
2. (a) Andersson, L.; Blomberg, L.; Flegel, M.; Lepsa, L.; Nilsson, B.; Verlander, M. *Biopolymers* **2000**, *5*, 227; (b) Bray, B. L. *Nat. Rev. Drug Disc.* **2003**, *2*, 587.
3. Dingermann, T. *Biotechnol. J.* **2008**, *3*, 90.
4. For recent reviews on the preparation of peptides and proteins having nonproteinogenic amino acid(s) or post-translational modification, see: (a) Muralidharan, V.; Muir, T. W. *Nat. Methods* **2006**, *3*, 429; (b) Bennett, C. S.; Wong, C. H. *Chem. Soc. Rev.* **2007**, *36*, 1227; (c) Ohta, A.; Yamagishi, Y.; Suga, H. *Curr. Opin. Chem. Biol.* **2008**, *12*, 159.
5. (a) Stark, G. R. *Methods Enzymol.* **1977**, *47*, 129; (b) Nakagawa, S.; Tamakashi, Y.; Hamana, T.; Kawase, M.; Taketomi, S.; Ishibashi, Y.; Nishimura, O.; Fukuda, T. *J. Am. Chem. Soc.* **1994**, *116*, 5513; (c) Nishimura, O.; Moriya, T.; Suenaga, M.; Tanaka, Y.; Itoh, T.; Koyama, N.; Fujii, R.; Hinuma, S.; Kitada, C.; Fujino, M. *Chem. Pharm. Bull.* **1998**, *46*, 1490; (d) Yang, Y.; Wu, J.; Watson, J. T. *J. Am. Chem. Soc.* **1998**, *120*, 5834; (e) Suenaga, M.; Itoh, T.; Miwa, M.; Koyama, N.; Hinuma, S.; Kitada, C.; Nishimura, O.; Fujino, M. *J. Chem. Soc., Perkin Trans. 1* **2000**, 1183; (f) Itoh, T.; Miwa, M.; Suenaga, M.; Ohtaki, T.; Kitada, C.; Nishimura, O.; Fujino, M. *J. Chem. Soc., Perkin Trans. 1* **2000**, 1333; (g) Nishimura, O.; Suenaga, M.; Yamada, T.; Itoh, T.; Koyama, N.; Wakimasu, M.; Ohtaki, T.; Kitada, C.; Fujino, M. *J. Chem. Soc., Perkin Trans. 1* **2001**, 1748; (h) Qi, J.; Wu, J.; Somkuti, G. A.; Watson, J. T. *Biochemistry* **2001**, *40*, 4531.
6. (a) Wu, J.; Watson, J. T. *Anal. Biochem.* **1998**, *258*, 268; (b) Tang, H. Y.; Speicher, D. W. *Anal. Biochem.* **2004**, *334*, 48.
7. Hayashi, Y.; Takayama, K.; Suehisa, Y.; Fujita, T.; Nguyen, J. T.; Futaki, S.; Yamamoto, A.; Kiso, Y. *Bioorg. Med. Chem. Lett.* **2007**, *17*, 5129.
8. Other side reactions including dimerization of the peptides by disulfide bond formation were also observed.
9. The cyclic imide formation with concomitant peptide bond cleavage in neutral and basic conditions was previously reported: (a) Geiger, T.; Clarke, S. *J. Biol. Chem.* **1987**, *262*, 785; (b) Patel, K.; Borchardt, R. T. *Pharm. Res.* **1990**, *7*, 787.
10. The ε-lactam formation accompanying amide bond cleavage was previously reported: (a) Takenawa, T.; Oda, Y.; Ishihama, Y.; Iwakura, M. *J. Biochem.* **1998**, *123*, 1137; (b) Ishihama, Y.; Ito, O.; Oda, Y.; Takenawa, T.; Iwakura, M. *Tetrahedron Lett.* **1999**, *40*, 3415.
11. A small amount of a β-elimination product was observed under the various cleavage conditions examined.
12. Otaka, A.; Nakamura, M.; Nameki, D.; Kodama, E.; Uchiyama, S.; Nakamura, S.; Nakano, H.; Tamamura, H.; Kobayashi, Y.; Matsuoka, M.; Fujii, N. *Angew. Chem., Int. Ed.* **2002**, *41*, 2937.
13. Only partial S-cyanylations of two Cys residues in thioredoxin were observed. This was also verified by the recovery of C-terminal capped thioredoxin **24a,b** after basic treatment in the next step.
14. Peptides **20a,b** from **22a,b** were identical to the authentic samples, which were obtained by the cleavage reaction of the synthetic peptides.
15. Cytotoxicity of peptides **20a,b** was not observed even at 10 μM in MAGI assay.
16. The presence of a hydrolyzed ring-opening product indicates that the degradation presumably began with hydrolysis of the C-terminal aspartimide, Ref. 9.
17. (a) Kodama, E. I.; Kohgo, S.; Kitano, K.; Machida, H.; Gatanaga, H.; Shigeta, S.; Matsuoka, M.; Ohrui, H.; Mitsuya, H. *Antimicrob. Agents Chemother.* **2001**, *45*, 1539; (b) Maeda, Y.; Venzon, D. J.; Mitsuya, H. *J. Infect. Dis.* **1998**, *177*, 1207.